The Multifaceted Role of EXOC6A in Ciliogenesis

Te-Lin Lin[1,2], Chien-Ting Wu[2,3], and Tang K. Tang[1,2,#]

1. Taiwan International Graduate Program in Molecular Medicine, National Yang Ming Chiao Tung University and Academia Sinica, Taipei, Taiwan
2. Institute of Biomedical Sciences, Academia Sinica, Taipei, Taiwan
3. Department of Microbiology, University of Texas Southwestern Medical Center, Texas, USA

Correspondence: Tang K. Tang, tktang@ibms.sinica.edu.tw

Abstract

Ciliogenesis is a highly ordered process that requires membrane trafficking, fusion, and maturation. In this study, we investigated EXOC6A, a component of the exocyst complex known for secretory vesicle trafficking and fusion, and found that it interacts with myosin-Va (Myo-Va) during ciliogenesis. EXOC6A colocalizes with Myo-Va at various stages of ciliogenesis, including preciliary vesicles, ciliary vesicles (CVs), and ciliary sheath membrane during ciliogenesis. We found that EXOC6A vesicles are actively recruited, integrated, and exit from the CVs and the ciliary sheath, implying that EXOC6A vesicles may facilitate continuous cilia membrane remodeling during ciliogenesis. Importantly, EXOC6A knockout impairs ciliogenesis, arresting most cells at the CV stage and preventing recruitment of NPHP and MKS module components to the transition zone. Furthermore, EXOC6A vesicles are transported to the mother centriole via a dynein-, microtubule-, and actin-dependent mechanism. Our results suggest that EXOC6A functions in both early and late stages of ciliogenesis and is involved in orchestrating vesicle dynamics, cilia membrane remodeling, and formation.

Keywords: Ciliogenesis, ciliary membrane assembly, intracellular pathway, exocyst complex, myosin-Va

Introduction

Most mammalian cells build primary cilia, which act as chemosensors or mechanosensors and as transducers that regulate key developmental signaling pathways. Primary cilia are composed of nine doublet microtubules arranged in a ring and surrounded by a ciliary membrane that is continuous with the plasma membrane (Dawe et al., 2007; Nigg and Raff, 2009). Primary cilia protrude from the cell surface to perform a wide range of biological functions. Defects in ciliogenesis can lead to a number of genetic disorders known as ciliopathies, which are characterized by loss of vision, disturbed kidney function, obesity, and defects in brain development (Sattar and Gleeson, 2011; Valente et al., 2014).

Ciliogenesis is a highly ordered and complex process. Currently, two distinct pathways have been reported, with different cell types involved: intracellular and extracellular. Polarized epithelial cells use the extracellular pathway, whereas fibroblasts and mesenchymal cells use the intracellular pathway (Breslow and Holland, 2019). In the intracellular pathway, myosin-Va (Myo-Va) facilitates the transportation of preciliary vesicles (PCVs) to the distal appendages (DAs) of the mother centrioles (Wu et al., 2018). These PCVs may be derived from the Golgi apparatus (Schmidt et al., 2012) and subsequently fuse with a ciliary vesicle (CV) through the action of membrane fusion regulators EHD1 and EHD3 (Lu et al., 2015).

This step is critical for the conversion of the mother centriole into a basal body, which is responsible for removing the centriole cap protein, CP110, and recruiting ciliary transition zone (TZ) proteins (Lu et al., 2015). As a result, an axoneme extends within the larger CV, which gradually stretches out to form the double membranes of the ciliary shaft and sheath that surround the extending axoneme. Finally, the ciliary sheath (the outer membrane) fuses with the plasma membrane and the axoneme, enveloped by the ciliary shaft membrane, extends from the cell membrane, and makes contact with the extracellular environment (Ghossoub et al., 2011). A signaling cascade including RAB11, RABIN8, and RAB8 has also been reported to regulate the ciliary membrane assembly (Chiba et al., 2013; Feng et al., 2012; Knödler et al., 2010; Nachury et al., 2007; Westlake et al., 2011; Yoshimura et al., 2007). However, the processes of formation of the ciliary sheath and ciliary shaft membrane during ciliogenesis remain unclear.

The exocyst is a multi-subunit protein complex that was first identified in yeast, which mediates the tethering of secretory vesicles to the plasma membrane (Mei and Guo, 2018). The complex is composed of eight subunits, named Sec (for secretion; Sec3, Sec5, Sec6, Sec8, Sec10, Sec15, Exo70, and Exo84) in yeast or Exoc (for exocyst-related; EXOC1 to 8) in humans (TerBush et al., 1996; TerBush and Novick, 1995).

The exocyst complex is implicated in various cellular processes, including exocytosis, ciliogenesis, cytokinesis, autophagy, cell polarity, migration, tumorigenesis, and fusion of secretory vesicles (Mei and Guo, 2018).

Mutations in genes encoding components of the exocyst complex have been associated with various human genetic disorders. For example, a mutation in *EXOC8* has been identified in Joubert syndrome (Dixon-Salazar et al., 2012), while a mutation in *EXOC4* has been reported in Meckel–Gruber syndrome (Shaheen et al., 2013). Both of these disorders involve clinically and genetically heterogeneous ciliopathy. Additionally, mutations in *EXOC2* cause severe defects in human brain development (Van Bergen et al., 2020), while mutations in *EXOC7* and *EXOC8* result in a novel disorder of cerebral cortex development, characterized by brain atrophy, seizures, developmental delay, and microcephaly (Coulter et al., 2020). However, the essential roles of these genes in ciliogenesis and their correlation with human genetic disorders are currently unknown.

It has been reported that some components of the exocyst complex are involved in ciliogenesis. For example, Sec10 (EXOC5) was shown to be required for ciliogenesis and cyst formation in vitro, and Sec10 knockdown leads to reduce ciliogenesis (Zuo et al., 2009; Zuo et al., 2019). Furthermore, other subunits such as EXOC3 and EXOC4 have been detected at the cilium with unknown function (Seixas et al., 2016). Interestingly, depletion of Sec8, Exo70, or Sec10 does not impair ciliogenesis (Rivera-Molina et al., 2021), whereas knockdown of Sec15a (EXOC6A) significantly perturbs ciliogenesis (Rivera-Molina et al., 2021). These findings imply that different exocyst subunits may have distinct, non-redundant functions during ciliogenesis. However, the precise localization of EXOC6A within cilia and its specific role in regulating ciliary membrane formation or trafficking events remain largely unknown.

Previously, we demonstrated that the earliest event in ciliogenesis is the transportation of PCVs by Myo-Va to the distal appendages of the mother centriole, and we showed that Myo-Va is released from the ciliary membrane upon fusion of the ciliary sheath with the plasma membrane (Wu et al., 2018). However, the mechanism of the assembly of double ciliary membranes (ciliary sheath and shaft) during intracellular ciliogenesis was left unknown. In this study, we provide evidence that the exocyst component EXOC6A interacts with Myo-Va and plays an essential role in ciliary membrane assembly at different stages during ciliogenesis.

104 # Results

105 **Colocalization patterns of EXOC6A and Myo-Va at preciliary vesicles, ciliary**
106 **vesicles, and ciliary sheath during intracellular ciliogenesis**

107 To investigate the localization of EXOC6A during ciliogenesis, we treated retinal
108 pigment epithelial (RPE1)-based mCherry-tagged Myo-Va cargo binding domain
109 (Myo-Va-GTD)-inducible cells with doxycycline (Dox) for 24 h and then serum starved
110 them for 2h to induce ciliogenesis. In this Tet-On system, Dox treatment triggers the
111 inducible expression of the mCherry-Myo-Va-GTD transgene. We used antibodies
112 against endogenous EXOC6A and glutamylated tubulin (Glu-tub), a marker of
113 centrioles and ciliary axoneme, for confocal immunofluorescence analysis. Our results
114 showed that the EXOC6A signal was mainly detected as a dot-shaped structure
115 resembling a ciliary vesicle (CV) at the distal end of the mother centriole (Fig. 1A, left),
116 while some EXOC6A signals appeared to be colocalized with mCherry-tagged Myo-
117 Va-GTD at the ciliary membrane (Fig. 1A. right). To determine the subcellular
118 localization of EXOC6A, we performed immunofluorescence staining using antibodies
119 against CEP164 (a distal appendage marker, (Graser et al., 2007)) and CEP120 (a
120 centriole marker, (Lin et al., 2013)). The PCV/CV/ciliary sheath can be visualized with
121 mCherry-tagged Myo-Va-GTD (Wu et al., 2018). The cells were then analyzed using
122 three-dimensional structured illumination microscopy (3D-SIM, Fig. 1B) or
123 ultrastructure expansion microscopy (U-ExM, Fig. 1C). Our results showed that
124 EXOC6A signals colocalized with mCherry-Myo-Va-GTD at CV (Fig. 1B and C). To
125 further define the position of the EXOC6A signal, we performed Correlative Light and
126 Electron Microscopy (CLEM) in RPE1-based GFP-EXOC6A-inducible cells (Fig. 1D).
127 Our CLEM results showed that the GFP-EXOC6A signals appeared to localize at PCVs
128 (or vesicles), CVs (Fig. 1D-i-ii), and the elongating ciliary membrane (Fig. 1D-iii-iv).

129 To precisely analyze the subcellular localization of EXOC6A and Myo-Va during
130 the formation of the ciliary sheath and the shaft membrane, we used 3D-SIM to analyze
131 the RPE1 cells that exogenously express inducible GFP-EXOC6A using known
132 markers combined for the ciliary sheath (Myo-Va-GTD; (Wu et al., 2018)), the ciliary
133 shaft (ARL13B, INPP5E; (Feng et al., 2012; Garcia-Gonzalo et al., 2015; Wu et al.,
134 2018), and the axoneme (Glu-tub). EXOC6A signals were commonly detected at the
135 Myo-Va-GTD-labeled ciliary sheath (Fig. 1E-i, ii), which surrounds the ciliary shaft
136 membrane (labeled ARL13B and INPP5E, Fig. 1E-i, iii) and the axoneme (Glu-tub, Fig.
137 1E-ii, iii). Since our 3D-SIM analysis could not distinguish the spatial distances
138 between INPP5E and the Glu-tub-labeled axoneme due to the limits of its resolution
139 power (100–130 nm), we thus conclude that EXOC6A localizes at the ciliary sheath

membrane surrounding the ciliary shaft. Altogether, our data show that EXOC6A, like Myo-Va, localizes at the PCVs, the CVs, and the ciliary sheath membrane.

Spatial and temporal localization of Myo-Va and EXOC6A during ciliogenesis

To investigate the temporal and spatial correlation between the ciliary localization of EXOC6A and Myo-Va during ciliogenesis, we used RPE1-based mCherry-Myo-Va-GTD-inducible cells that were serum starved, released at different time points, and analyzed using 3D-SIM with antibodies against endogenous EXOC6A and Glu-tub (Fig. 2A). We identified five different phenotypes based on the immunostaining patterns of Myo-Va and EXOC6A during cilium assembly (Fig. 2B), which are quantified in Fig. 2C. Before serum starvation, a number of EXOC6A-associated vesicles were detected close to the mother centriole (Fig. 2A, 0 min, type 1). During the progression of serum starvation, EXOC6A-associated vesicles appeared to gradually accumulate near the mother centriole (Fig. 2A, 15 min, type 2) in a process we called "clustering-to-centriole," and subsequently, EXOC6A signals were mainly detected at the Myo-Va-labeled CVs (Fig. 2A, 30 min–1 h, type 3) and the ciliary sheath membrane, surrounding the Glu-tub-labeled axoneme (Fig. 2A, 2 h, type 4). In some cells, a tubule-like structure ($EXOC6A^+$/$Myo\text{-}Va^+$) linked to the ciliary sheath membrane was observed (Fig. 2A, 4 h, white arrow). Finally, both EXOC6A and Myo-Va were released from the ciliary sheath membrane when it fused to the plasma membrane, while the Glu-tub-labeled axoneme continued to protrude into the extracellular milieu (Fig. 2A, 24 h, type 5). Interestingly, we observed that only a portion, but not all of the EXOC6A-labeled vesicles colocalized with Myo-Va-labeled PCVs (Fig. 2A, 0 and 15 min). However, once the CVs formed, both EXOC6A and Myo-Va-GTD signals were detected at the CVs (Fig. 2A, 30 min, 45 min, and 1 h). We present a schematic model in Figure 2B that shows the localization of EXOC6A (green) and mCherry-Myo-Va-GTD (red) during ciliogenesis and the types of immunostaining patterns.

To further understand the relationship between the clustering-to-centriole progression of EXOC6A and Myo-Va during the early stage of ciliogenesis, we analyzed the intensity of both proteins clustering to the centrioles and calculated their overlapping co-efficiency correlation R (Pearson correlation coefficient) using Zeiss Zen software (Fig. S1). We observed a gradual increase in the mean intensity of EXOC6A and Myo-Va clustering to the centrioles from 0 to 30 min (Fig. S1A–C). Additionally, the correlation R between EXOC6A and Myo-Va significantly increased from 0 to 30 min (Fig. S1D). These results suggest a high correlation between Myo-Va-labeled vesicles and EXOC6A-labeled vesicles during the progression of clustering-to-centriole.

FRAP analysis of the dynamic localization of Myo-Va- and EXOC6A-labeled

178 **vesicles during ciliogenesis**

179 We found that some EXOC6A structures had a tubule-like structure extending from
180 the ciliary sheath (Fig. 2A, 4 h, type 4), suggesting the dynamic assembly of the ciliary
181 membrane during ciliogenesis. To gain further insights into the dynamic relationship
182 between Myo-Va- and EXOC6A-labeled vesicles during early CV formation and the
183 later sheath membrane assembly stage, we performed live cell imaging with
184 fluorescence recovery after photobleaching (FRAP). FRAP is a widely used technique
185 to measure the dynamics of ciliary membrane protein localization (Kee et al., 2012;
186 Westlake et al., 2011). After photobleaching at CVs or the ciliary sheath region, the
187 EXOC6A signals were recurrently recruited to the CVs (Fig. 3A, Movie 1) and the
188 ciliary sheath membrane within seconds (Fig. 3B, Movie 2). Together, our data
189 indicated that the EXOC6A-labeled vesicles are continuously recruited to and fused
190 with the ciliary membrane not only at the CVs but also at the ciliary sheath. To further
191 investigate the dynamic properties of the ciliary membrane, we performed live-cell
192 super-resolution imaging using the ELYRA 7 SIM system. We used SiR-tubulin, a
193 fluorescent probe derived from the microtubule-stabilizing drug docetaxel, to label
194 endogenous microtubules. This allowed us to visualize the structure of centrioles and
195 axonemes during ciliogenesis in live imaging experiments (Fig. S2). Our results show
196 that EXOC6A co-localizes with Myo-Va-GTD on the ciliary membrane and surrounds
197 the SiR-tubulin-labeled axoneme (Fig. S2A and S2B). In addition, we detected a
198 dynamic tubule-like structure that extended and retracted from the ciliary membrane
199 (Fig. S2A, S2C, and Movie 3). To better observe vesicle trafficking and membrane
200 dynamics, we used the single-channel and burst modes of the ELYRA 7 SIM system to
201 achieve higher temporal resolution in live imaging. Our results showed that GFP-
202 EXOC6A-labeled vesicles gradually moved to and fused with CVs (Fig. 3C, white
203 arrow; Movie 4) and the ciliary pocket, a membrane domain found at the base of
204 primary cilia (Fig. 3D, white arrow, Movie 5). Interestingly, almost at the same time,
205 some GFP-EXOC6A-labeled vesicles were fused with or secreted from the ciliary
206 pocket (Fig. 3D, red arrow, Movie 5). Unexpectedly, we observed that some GFP-
207 EXOC6A-associated tubular structures (Fig. 3D, yellow arrow) or GFP-EXOC6A-
208 labeled vesicles were released directly from the ciliary membrane rather than from the
209 ciliary pocket (Fig. 3D, orange arrow). Together, our results indicate that GFP-
210 EXOC6A-associated vesicles/membranes are highly dynamic and continuously
211 recruited to and/or released from CVs during the early stages of ciliogenesis, and that
212 they are also fused with or excreted from the ciliary membrane during later stages of
213 ciliogenesis. We, therefore, propose that EXOC6A vesicles are responsible for the
214 exchange of materials within existing CVs and the ciliary sheath during ciliogenesis,
215 facilitating the addition or removal of membranes or membrane proteins.

216 **Myo-Va and EHD1 are required for EXOC6A-labeled CV formation, and**
217 **EXOC6A is associated with Myo-Va**

218 We previously reported that Myo-Va-mediated transportation of PCVs to the mother
219 centriole is the earliest event that defines the onset of ciliogenesis (Wu et al., 2018). In
220 this study, we aimed to examine the sequential order of PCV transportation mediated
221 by Myo-Va and EXOC6A during ciliogenesis in both RPE1-based *Myo-Va* knockout
222 (KO) and *EXOC6A* KO cells. We constructed two independent *EXOC6A* knockout (KO)
223 cell lines using the CRISPR–Cas9 system. The success of the gene disruption was
224 validated at the genomic level through target site sequencing (Fig. S3A), a schematic
225 diagram of predicted peptide products (Fig. S3B), and Western blot analysis (Fig. S3C),
226 confirming the absence of EXOC6A expression in all KO cell lines. All independent
227 KO cell lines exhibited similar ciliary generation defects (Fig. S3D). The EXOC6A
228 signal is located at CV (Fig. S3E) and cilia sheath (Fig. S3F), but is absent in both
229 *EXOC6A* KO cell lines. Our results showed that few EXOC6A-labeled vesicles and no
230 EXOC6A-labeled CVs were detected at the distal end of the mother centriole in the
231 *Myo-Va* KO cells (Fig. 4A). In contrast, Myo-Va-labeled CVs were frequently observed
232 at the mother centrioles of *EXOC6A* KO cells (Fig. 4B). Similar results were also
233 observed in the other *EXOC6A* KO cell line. Together, our findings suggest that
234 EXOC6A is not essential for the formation of Myo-Va-labeled CVs during ciliogenesis.
235 EHD1 was reported to be essential for the fusion of PCVs to form larger CVs during
236 the early stage of ciliogenesis (Lu et al., 2015). To investigate the sequential order of
237 EHD1- and EXOC6A-mediated ciliary membrane assembly, we depleted EHD1
238 expression using siRNA in RPE1 cells. Our results showed that EHD1 depletion led to
239 a reduction in the formation of EXOC6A-labeled CVs (Fig. 4C). In contrast, *EXOC6A*
240 KO did not appear to affect EHD1-mediated fusion of PCVs to form a large EHD1-
241 labeled CV at the mother centriole (Fig. 4D). Together, our findings suggest that EHD1
242 is required for EXOC6A-labeled CV formation, while EXOC6A is not essential for the
243 formation of EHD1-labeled CVs
244 Additionally, previous studies reported that Myo2p, the yeast homolog of human
245 Myo-Va, interacts with sec15, the yeast homolog of human EXOC6A (Jin et al., 2011).
246 The present study showed that some, but not all of the EXOC6A-labeled PCVs
247 colocalized with Myo-Va-labeled PCVs (Fig. 2A, 0 and 15 min). We speculate that
248 Myo-Va may transport some EXOC6A-labeled vesicles to the CVs for ciliary
249 membrane assembly. Our co-immunoprecipitation experiments showed that
250 endogenous EXOC6A can co-immunoprecipitate with Myo-Va, supporting this
251 hypothesis (Fig. 4E).

252 Finally, previous studies have indicated that the removal of centriolar protein CP110
253 from the distal end of the mother centriole is necessary for axoneme growth (Spektor
254 et al., 2007). It has been proposed that CP110 removal occurs after the docking of CV
255 to the DA of the mother centriole (Lu et al., 2015; Wu et al., 2018). To investigate the
256 impact of EXOC6A loss on CP110 removal, we examined CP110 localization in
257 *EXOC6A* KO cells. Our results showed that CP110 is appropriately removed from the
258 distal end of the mother centriole in *EXOC6A* KO cells, indicating that EXOC6A is not
259 required for this process (Fig. S4), which further support that EXOC6A is not essential
260 for CV formation. Taken together, our findings suggest that Myo-Va transports a subset
261 of EXOC6A-labeled vesicles to the existing CVs of the mother centriole for ciliary
262 membrane assembly. However, EXOC6A is not essential for CV formation.
263

264 **Transportation of EXOC6A-labeled vesicles to the mother centriole is via a**
265 **dynein-, MT-, and Arp2/3-dependent pathway**

266 Our previous study showed that the transportation of PCVs to the distal appendages
267 of the mother centriole is mediated by Myo-Va, dynein, microtubules (MTs), and the
268 Arp2/3 complex (Wu et al., 2018). In the current study, we found that Myo-Va and
269 EHD1 are required for EXOC6A-labeled CV formation and that Myo-Va co-
270 immunoprecipitates with EXOC6A (Fig. 4). It has been reported that dynein is
271 necessary for the correct positioning of the Golgi complex near the centrosome upon
272 serum starvation (Palmer et al., 2009; Wu et al., 2018), and that the inhibition of dynein
273 activity with ciliobrevin D suppresses ciliogenesis (Firestone et al., 2012; Wu et al.,
274 2018). Therefore, we investigated whether the transport of EXOC6A-associated
275 vesicles to the DA of the mother centriole also requires dynein, MTs, and the Arp2/3
276 complex.
277 RPE1 cells were transfected with siRNAs targeting Golgin160, a protein required for
278 the recruitment of dynein to the Golgi complex (Yadav et al., 2012), or treated with
279 ciliobrevin D, a known cytoplasmic motor dynein inhibitor that suppresses ciliogenesis
280 (Firestone et al., 2012), following the protocol described in Figure 5A. Our findings
281 showed that depletion of Golgin160 led to a decrease in EXOC6A-labeled CV signals
282 at or near the mother centriole (Fig. 5B, D) and resulted in the dispersion of Golgi
283 matrix protein 130 (GM-130)-labeled Golgi complexes (Fig. 5B, E), ultimately leading
284 to a reduction in the total number of cilia (Fig. 5F). Similar results were also observed
285 in RPE1 cells treated with 10 μM ciliobrevin D (Fig. 5C-i, D–F). We next treated RPE1
286 cells with 10 μM nocodazole (NZ, an MT-depolymerizing drug) and examined its effect
287 on ciliogenesis. Our results showed that the EXOC6A-labeled CVs and the cilia number
288 are greatly reduced in NZ-treated cells (Fig. 5C-ii, D, and F). These data suggest that a

289 subset of EXOC6A-positive vesicles may originate from the Golgi apparatus.
290 Furthermore, the accumulation of these vesicles at the mother centrioles is highly
291 sensitive to disruption of dynein or microtubules, suggesting that efficient transport of
292 these vesicles may depend on the integrity of the microtubule network. However, more
293 experiments are required to confirm this conclusion.

294 Since Myo-Va-mediated transport of PCVs to the mother centrioles relies on an
295 Arp2/3-dependent branched actin network surrounding mother centrioles (Wu et al.,
296 2018), we next treated RPE1 cells with siARP2 (Fig. 5G). A reduced cilia number (Fig.
297 5G and H) and reduced EXOC-6A-labeled CVs (Fig. 5G and I) were observed in
298 siARP2-treated cells. A similar result was also found in cells treated with 200 μM
299 CK666 (a known specific Arp2/3 inhibitor) or high-dose (10 μM) cytochalasin D
300 (CytoD), which has been reported to reduce the association of ARP2 with the branched
301 actin network (Fig. 5H–J). It has been reported that low concentrations (100 nM-1 μM)
302 of CytoD can promote ciliogenesis and increase cilia length (Cao et al., 2023; Kim et
303 al., 2015; Kim et al., 2010; Wu et al., 2018), while high concentrations (10 μm) lead to
304 a significant inhibition of cilia formation (Wu et al., 2018). To further investigate the
305 dose-dependent effects of actin cytoskeleton rearrangement on ciliogenesis, we treated
306 RPE1 cells with CytoD at concentrations ranging from 200 nM to 10 μM.
307 Immunofluorescence staining of cilia using ARL13B (green) and Glu-tubulin (red)
308 antibodies showed that low concentrations of CytoD (200 nM–2 μM) resulted in
309 significant cilia elongation, whereas higher doses (4 μM, 7μM and 10μM) gradually
310 inhibited cilia formation (Fig. S5). Consistent with our previous findings (Wu et al.,
311 2018), our data showed that cilia length and cilia ratio increased at low doses of CytoD
312 (200 nM-2 μM) but gradually decreased with increasing doses (7 μM and 10 μM, Fig.
313 S5B and C).

314 Taken together, our current studies reinforce our previous view (Wu et al., 2018) that
315 low-dose of CytoD treatment (200 nM-2 μM) can stabilize and/or enhance the
316 formation of Arp2-associated branched actin filaments. However when cells were
317 treated with high doses of CytoD (7 μM and 10 μM, Fig. S5) or the specific Arp2/3
318 inhibitor, CK-666 (Fig. 5), the association of Arp2 with the branched actin network was
319 significantly reduced, thereby inhibiting ciliogenesis. In conclusion, our data suggest
320 that Myo-Va carries EXOC6A vesicles to the DA of mother centriole via a dynein-,
321 microtubule-, and actin-dependent pathway.
322

323 **Loss of EXOC6A inhibits ciliogenesis, and some cells exhibit abnormal ciliary**
324 **morphology when passing through the CV block**

325 We found that EXOC6A signals are detected at CVs and the ciliary sheath (Fig. 1

326 and 2). We also found that EXOC6A-associated vesicles are dynamically recruited to
327 or excreted from CVs and/or the ciliary membrane (Fig. 3). We next examined the
328 effects of *EXOC6A* deletion on ciliogenesis. As shown in Figure 6, *EXOC6A* KO
329 significantly inhibits cilia assembly, resulting in either no cilia or dotted CV signals
330 after serum starvation (SS, 30 min–48 h). Upon serum starvation for 30 min, Myo-Va-
331 GTD-labeled CVs were detected at the mother centriole in both wild-type control (Fig.
332 6A) and *EXOC*6A KO cells (Fig. 6A'). In control cells, the Myo-Va-GTD signal was
333 mainly detected at the ciliary sheath membrane (Fig. 6A, SS 2h) 2 h after serum
334 starvation, while the Myo-Va-GTD signals dissociated from the ciliary sheath
335 membrane after longer starvation (SS 24 h or SS 48 h). Interestingly, most Myo-Va-
336 GTD signals in *EXOC6A* KO cells were present as dotted CVs after longer starvation
337 (SS 48 h), suggesting that ciliogenesis is arrested at the CV stage (Fig. 6A').
338 We next used an antibody against ARL13B (a cilia shaft marker) to label the ciliary
339 membrane and found that most *EXOC6A* KO cells exhibited no cilia (~45%, Fig. 6C)
340 or dotted ARL13B signals (~50%) 2 h after SS (Fig. 6B'; Fig. 6C, SS 2 h), a pattern
341 similar to Myo-Va staining (Fig. 6A'). Unexpectedly, after prolonged serum starvation,
342 we could still detect approximately ~15% (SS 24 h) to ~30% (SS 48 h) of *EXOC6A* KO
343 cells carrying ARL13B-labeled cilia protruding from the basal body. However, these
344 ARL13B-labeled cilia showed a low intensity of ARL13B and Glu-tub signals (Fig. 6D
345 and E) and the ARL13B-labeled cilia membrane exhibited a fragmented and punctuated
346 staining pattern (enhanced in Fig. 6B, SS 48 h in lower panel). Our findings suggest
347 that EXOC6A may play a crucial role in the further maturation of CVs into the ciliary
348 sheath/shaft membrane during ciliogenesis.
349 To examine whether EXOC6A is required for ciliogenesis and whether its function
350 can be rescued, we analyzed cilia formation in wild-type (WT), EXOC6A KO, and
351 EXOC6A KO cells exogenously expressing GFP-EXOC6A. Immunofluorescence
352 staining of cells with ARL13B and Glu-tubulin antibodies showed a significant
353 reduction in the number of cilia in EXOC6A KO cells. Importantly, exogenous
354 expression of GFP-EXOC6A in the KO cells resulted in a statistically significant
355 recovery of the ciliated cell population (*P=0.0041)* and a concomitant reduction in
356 stalled vesicles, confirming that this phenotype was caused by EXOC6A loss. (Fig. S6).
357 Electron microscopy was further used to investigate the cilia morphology in the
358 *EXOC6A* KO cells after prolonged serum starvation (72 h). To examine ciliary structure
359 in *EXOC6A* KO cells in more detail, we used a 72 h-serum starvation protocol, which
360 provided sufficient time for cilia assembly. Our results showed a perturbation in cilia
361 assembly in *EXOC6A* KO cells (Fig. 6F and G). When compared with the wild-type
362 control (Fig 6F-i and ii), cilia in *EXOC6A* KO cells exhibited some ciliogenic defects,
363 such that ciliogenesis was often arrested at the DA/PCV or CV stage (Fig. 6F-iii and

364 iv), and some exhibited morphologically curved cilia bending in the TZ region (Fig.
365 6F-vi, 4/37 in Fig. 6G). Intriguingly, a small proportion of KO cells produced an
366 elongated large CV in the absence of an extended axoneme (Fig. 6F-v, 4/37 in Fig. 6G).
367 Consistent with this finding, curved cilia (Fig. 6B, SS 24 h, lower panel) and a low
368 intensity of Glu-tub-labeled axoneme were observed in *EXOC6A* KO cells via confocal
369 immunofluorescence microscopy (Fig. 6B, SS 48 h, lower panel. Fig. 6E). Nonetheless,
370 we still observed 3 out of 37 morphologically normal-like cilia in *EXOC6A* KO cells
371 (Fig. 6F-vii, 6G). Taken together, our data suggest that depletion of EXOC6A primarily
372 affects cells exhibiting no CV (showing only DA/PCV; Fig. 6F-iii, Fig. 6G) and/or
373 arrests cells at the CV stage, while once it passes through CV stage after prolonged
374 serum starvation, it may interfere with subsequent cilia membrane formation at later
375 stages of ciliogenesis.
376

377 **EXOC6A is required to recruit NPHP and MKS module components to the TZ**
378 **and GPR161 and BBS9 to the ciliary membrane**

379 Our EM study revealed both bending cilia at the TZ (4/37, Fig. 6G-vi) and
380 morphologically normal-like cilia (3/37, Fig. 6G-vii). Intriguingly,
381 immunofluorescence analysis revealed that the ARL13B signal intensity was greatly
382 reduced in the normal-like cilia membrane in *EXOC6A* KO cells (Fig. 6D), suggesting
383 a possible defect in the TZ of cilia. The TZ is a diffusion barrier at the ciliary membrane
384 that acts as a gate to regulate the entry and exit of ciliary proteins required for signal
385 transduction (Jensen and Leroux, 2017). Previous studies have identified three
386 conserved protein modules (MKS, NPHP, and CEP290), composed of numerous
387 protein complexes that cooperate in the assembly and gating function of the TZ
388 (Gonçalves and Pelletier, 2017). CEP290, located at a proximal position near the
389 mother centriole, acts as a hub that interacts with the NPHP and MKS module
390 complexes (Garcia-Gonzalo and Reiter, 2017).
391 To verify the integrity of these abnormal cilia in *EXOC6A* KO cells, we
392 examined the recruitment of several known TZ proteins, including CEP290, NPHP, and
393 MKS module proteins. Our results showed that the recruitment of CEP290 to the ciliary
394 base was normal in all examined ciliated cells, indicating that EXOC6A deletion did
395 not affect CEP290 targeting to the TZ (Fig. 7A). However, the recruitment of several
396 MKS complex proteins (TCTN2, AHI1, MKS3, and MKS1) to the basal body (mother
397 centriole) was severely impaired in *EXOC6A* KO ciliated cells (Fig. 7B), while NPHP8
398 recruitment was only partially affected (Fig. 7B). Collectively, our findings suggest that
399 EXOC6A is not required for CEP290 targeting to the TZ but plays an essential role in
400 the recruitment of several NPHP and MKS module proteins to the basal body, which

401 potentially affects the gating function of the TZ in *EXOC6A* KO cells.
402 We next investigate whether the EXOC6A deficiency affects the transport of ciliary
403 membrane proteins, we examined the localization of GPR161 and BBS9 in *EXOC6A*
404 KO cells. GPR161 is a G-protein-coupled receptor that negatively regulates the Sonic
405 hedgehog (Shh) signaling pathway (Mukhopadhyay et al., 2013), while BBS9 is a core
406 component of the BBSome complex and is essential for cilia homeostasis (Wingfield
407 et al., 2018). Our results showed that both GRP161 and BBS9 were properly recruited
408 to the cilia in WT cells (Fig. 7C). However, in *EXOC6A* KO cells, the entry of these
409 proteins into the ciliary compartment was completely blocked (Fig. 7C). Our findings
410 suggest that EXOC6A is essential for the recruitment of a subset of TZ proteins and
411 membrane proteins to the cilia during ciliogenesis.
412
413

Discussion

Cilia assembly is a complex, multistep process involving the accumulation and attachment of PCVs at the distal appendage, CV formation, and the subsequent extension of CVs into the ciliary sheath, alongside the formation of the ciliary shaft, ultimately leading to the mature cilia structure (Breslow and Holland, 2019; Long and Huang, 2019; Nachury et al., 2010). Currently, our understanding of the molecular mechanisms governing these steps remains incomplete. Exocytosis is a process where intracellular secretory vesicles fuse with the plasma membrane, aiding in delivering integral membrane proteins to the cell surface and releasing materials into the extracellular space (Martin-Urdiroz et al., 2016). Human EXOC6A exhibits a high degree of similarity to the product of the Saccharomyces cerevisiae *SEC15* gene. In yeast, SEC15 is essential for the movement of vesicles from the Golgi apparatus to the cell surface (Bowser and Novick, 1991). Previous studies have indicated that SEC15 interacts with Myo2p (the yeast homolog of human Myo-Va) and plays a role in vesicle exocytosis (Donovan and Bretscher, 2012; Donovan and Bretscher, 2015). Recently, exocyst was found to mediate the recycling of internal cilia and depletion of EXOC6A/Sec15a, but not other exocyst components, leads to a reduction in ciliogenesis (Rivera-Molina et al., 2021). This finding suggests that EXOC6A may have a unique function for ciliogenesis. However, the relationship and underlying mechanism between EXOC6A and Myo-Va in the context of ciliogenesis remain unclear.

In this study, we elucidated the role of the exocyst component EXOC6A in ciliogenesis and produced evidence for the model by which Myo-Va mediates trafficking of EXOC6A vesicles to the DA or existing CV of mother centriole in the early stages and to the ciliary membrane in the later stages of ciliogenesis (Fig. 8). However, further investigation will be required to fully establish the proposed hierarchy and molecular details. In this model, we found that a subset of EXOC6A-positive signals colocalized with Myo-Va-labeled signals during the early phase of ciliogenesis, and that they exhibited a high correlation during clustering-to-centriole progression after initiating ciliogenesis (Fig. S1A-D). Intriguingly, not all EXOC6A-labeled signals were positive for Myo-Va (Fig. 2A), suggesting the presence of at least two populations of Myo-Va-labeled vesicles in cells: one that is EXOC6A+/Myo-Va+ and another that is EXOC6A-/Myo-Va+ (Fig. 2A and Fig. 8).

In this model, ciliogenesis begins shortly after serum-starvation-induced quiescence. Initially, Myo-Va mediates the transport of PCVs (EXOC6A-/Myo-Va+ and EXOC6A+/Myo-Va+ vesicles) to the DA of the mother centriole, followed by the formation of PCVs to a CV via EHD1 (Lu et al., 2015; Wu et al., 2018). However,

451 EXOC6A is not absolutely required for CV formation, as *EXOC6A* KO did not interfere
452 with the formation of Myo-Va- or EHD1-labelled CV (Fig. 4B, 4D). Once the CV is
453 formed, the transport of EXOC6A vesicles to the existing CV in the early stages of
454 ciliogenesis is still mediated by Myo-Va (Fig. 4A). The above process involves a two-
455 step transportation mechanism: initially, dynein mediates the movement of Myo-Va-
456 associated vesicles (either EXOC6A-positive or EXOC6A-negative) towards the
457 pericentrosomal region along microtubules (MTs) (Fig. 5B–F). Subsequently, Myo-Va
458 takes over and drives these vesicles (EXOC6A-positive or -negative) from the
459 pericentrosomal region to the DAs of the mother centriole. This process is
460 accomplished through the utilization of the ARP2/3-associated branched actin network
461 (Fig. 5G–J). Notably, both of these Myo-Va-labeled vesicles require the function of
462 EHD1 to form a CV (Fig. 4D; Wu et al., 2018). Our findings that EHD1 depletion (Fig.
463 4D) and *Myo-Va* KO (Fig. 4A) severely impaired the formation of EXOC6A-positive
464 CVs at the mother centriole, suggest that Myo-Va and EHD1 play a role in promoting
465 the formation of EXOC6-positive CVs during the early stages of ciliogenesis.
466 Although EXOC6A is not absolutely required for the initial CV formation (Fig. 4B,
467 4D), our data revealed another role of EXOC6A in the later stages of ciliogenesis. Our
468 FRAP analysis and live cell imaging showed that a subset of EXOC6A-labeled vesicles
469 displayed high dynamism throughout ciliogenesis, continually being recruited to,
470 fusing into, or exited from existing CVs in the early stages and/or the ciliary membrane
471 (or ciliary pocket) in the later stages of ciliogenesis (Fig. 3). These EXOC6A-positive
472 vesicles, likely derived from the Golgi or recycling endocytic vesicles, are transported
473 to the ciliary membrane (or ciliary pocket) and/or fused with/exited from the ciliary
474 membrane in the later stages of ciliogenesis. The exocyst has been implicated in the
475 transport of vesicles carrying ciliary proteins to the cilia (Wu and Guo, 2015). Thus,
476 our findings suggested a potential role of EXOC6A vesicles, which may supply or
477 remove proteins or lipid moieties from the CVs and/or the ciliary membrane (or ciliary
478 pocket) during ciliogenesis.
479 Additionally, our results showed that *EXOC6A* KO led to the majority of the cells
480 being arrested at the CV stage or exhibiting no or few cilia (Fig. 6C); only a small
481 proportion of cilia were able to elongate, exhibiting an abnormal ciliary morphology
482 (Fig. 6B, 6F). Electron microscopic analysis of these abnormal cilia revealed elongated
483 CV (lacked axoneme, Fig. 6F-v), curved cilia bending at the TZ region (Fig. 6F-vi), or
484 normal-like cilia (Figure 6B-vii, whose structure and membrane composition need to
485 be further characterized). Further confocal immunofluorescence analysis revealed a
486 curved ciliary morphology (Fig. 6B, SS24h) and impaired recruitment of several known
487 TZ proteins, including TCTN2, AHI1, MKS3, and MKS1, to the basal body in *EXOC6A*
488 KO cells (Fig. 7). Taken together, our findings suggest that EXOC6A is required for the

489 early and the later stages of ciliogenesis as providing or removing ciliary components
490 (proteins or membrane moieties) to the existing CV or ciliary membrane, which
491 highlights its multifaceted involvement in the process of ciliary membrane formation.
492 Furthermore, the Rab11–Rabin8–Rab8 signaling pathway, which involves the
493 recruitment of Rabin8 (a GDP–GTP exchange factor for Rab8) and subsequent
494 activation of Rab8, has been implicated in ciliary membrane assembly (Knödler et al.,
495 2010; Nachury et al., 2007; Westlake et al., 2011; Yoshimura et al., 2007). Recently,
496 RAB34, located at the ciliary sheath (Ganga et al., 2021; Stuck et al., 2021), was also
497 reported to be required for ciliogenesis (Xu et al., 2018). The relationship between
498 EXOC6A, Rab11 signaling, and RAB34 in ciliogenesis is not clear. Future experiments
499 dissecting the underlying mechanisms between Rab11 signaling, RAB34, and
500 EXOC6A could provide a more complete picture of ciliary membrane assembly during
501 ciliogenesis.
502 Finally, ciliopathy-associated genes have been demonstrated to impact various stages
503 of mouse cortical development (Guo et al., 2015), and severe human ciliopathies are
504 linked to developmental abnormalities in the forebrain (Andreu-Cervera et al., 2021).
505 Mutations or deletions in genes encoding exocyst proteins, including *EXOC2*, *EXOC4*,
506 *EXOC7*, and *EXOC8*, have been associated with ciliopathies and neural developmental
507 disorders (Coulter et al., 2020; Dixon-Salazar et al., 2012; Shaheen et al., 2013;
508 Turkyilmaz et al., 2021; Van Bergen et al., 2020). Interestingly, deletions involving the
509 5' portion of the *EXOC6A* gene and two adjacent cytochrome p450 genes (*CYP26A1*
510 and *CYP26C1*) are associated with autosomal-dominant nonsyndromic optic aplasia
511 (ONA), an extremely rare disorder that causes unilateral or bilateral blindness in the
512 affected eye (Meire et al., 2011). The molecular basis remains unclear. Further studies
513 are needed to explore the specific roles of various types of ciliary vesicles, the
514 underlying mechanisms of their trafficking/fusion, and their relevance to ciliopathies
515 and neural developmental disorders.
516 In summary, we have identified a novel role for EXOC6A in ciliogenesis and
517 determined that it is essential for both early and late stages of this process. EXOC6A
518 vesicles may transport proteins or lipid moieties to and from the CV (early phase) and
519 the ciliary pocket/ciliary membrane (late phase) during ciliogenesis. However,
520 EXOC6A is not absolutely necessary for the initial CV formation; its function may be
521 to help assemble the complete transition zone and promote the maturation of existing
522 CVs into the ciliary sheath/shaft membrane. Furthermore, transportation of EXOC6A
523 vesicles to the mother centriole is mediated by Myo-Va and occurs via a dynein-, MT-,
524 and Arp2/3-dependent pathway. Our study provides new insights into the function of
525 EXOC6A in cilia membrane assembly during ciliogenesis. Future studies are needed to
526 explore the specific roles of different types of ciliary vesicles, the underlying

527 mechanisms of their trafficking and fusion, and their relevance to ciliopathies and
528 neural developmental disorders.
529

530 # Methods

531 **Plasmids and antibodies**

532 cDNAs encoding full-length EXOC6A were obtained via RT–PCR using total
533 RNAs from human HEK293T cells and subcloned in-frame into pcDNA4/TO/myc-His-
534 A (Invitrogen) or pLVX-Tight-Puro (BD Biosciences Clontech) GFP expression vectors.
535 GFP- and mCherry-myosin-Va-GTD constructs have been previously described (Wu et
536 al., 2018). The sequences of all constructed plasmids were confirmed.
537 Commercial antibodies used were anti-Sec15 (clone [15S2G6], 1/100 for IF,
538 Kerafast), anti-EXOC6 (1/100 for IF and 1/2000 for WB, Novus), anti-EXOC5 (1/2000
539 for WB, Proteintech), anti-EXOC7 (1/2000 for WB, Proteintech), anti-
540 polyglutamylated tubulin (Glu-tub, GT335, 1/100 for IF, AdipoGen), anti-CEP164
541 (1/500 for IF, Novus), anti-GFP (Abcam and Clontech), anti-ARL13B (1/600 for IF,
542 Proteintech), anti-myosin-Va (1/500 for IF and 1/5000 for WB, Novus), anti-EHD1
543 (1/500 for IF and 1/5000 for WB, Novus), anti-GM130 (1/1000 for IF, Abcam), anti-
544 CP110 (1/600 for IF, Proteintech), anti-Golgin160 (1/2000 for WB, Novus), anti-Arp2
545 (1/1000 for WB, Abcam), anti-TMEM67 (MKS3, 1/400 for IF, Proteintech), anti-
546 TCTN2 (1/400 for IF, Proteintech), anti-AHI1 (1/400 for IF, Proteintech), anti-MKS1
547 (1/400 for IF, Proteintech), anti-BBS9 (1/400 for IF, Proteintech), and anti-GPR161
548 (1/400 for IF, Proteintech). The secondary antibodies were Alexa 488/568/647
549 conjugated anti-mouse or rabbit (Invitrogen). The rabbit polyclonal antibody against
550 CEP120 (residues 639–986) was as described in our previous paper (Lin et al., 2013;
551 Tsai et al., 2019).

552 **Cell culture and cell lines**

553 Human telomerase-immortalized retinal pigment epithelial cells (RPE1) (Wu et al.,
554 2018) originally obtained from ATCC were maintained in DMEM/F12 (1:1)
555 supplemented with 10% FBS. Cells were transfected with various cDNA constructs
556 using TransIT-LT1 Transfection Reagent (Mirus). All cell lines were tested for
557 mycoplasma contamination and found negative.
558 The gRNA expression plasmids were obtained from Addgene (Addgene plasmid #
559 48138; http://n2t.net/addgene:48138 ; RRID:Addgene_48138), having been generated
560 by inserting annealed primers into the gRNA cloning vector pSpCas9-2A-GFP (PX458)
561 (Ran et al., 2013). The targeting sequences for the EXOC6A gRNA (gRNA1:5′-

562 TTGTATCCGTAATCATGACA -3′ ,gRNA2:5′- AAGTTACTGATACCAACCGA -3′
563 and gRNA3:5′- ACAAGTTTAACTCACCAGGAAGG -3′) primer pair purchased from
564 Mission Biotech were annealed and cloned into PX458. For transfection, 2.5 μg gRNA
565 (PX458 plasmid) was transfected with LT-1 reagent (Mirus) into RPE1 cells, according
566 to the manufacturer's instructions. The KO-1 clone was generated using a single-guide
567 RNA strategy (Fig. S3A-a). The PX458 vector encoding gRNA1, targeting exon 2 of
568 the EXOC6A gene, was transfected into RPE1 cells. The KO-2 independent clone was
569 generated using a dual-guide RNA strategy to induce a wider range of deletion (Fig.
570 S3A-b). Vectors encoding gRNA2 and gRNA3, targeting the flanking regions of exon
571 3 to exon 4, were co-transfected into cells. The transfected cells were sorted into single
572 cells (96-well plates) using a cell sorter (FACSAria, BD Biosciences) based on GFP
573 signal and then amplified. To confirm the depletion of EXOC6A, genomic DNAs
574 isolated from *EXOC6A* knockout colonies were subjected to PCR using the following
575 primers: and 5′- ACATCTCCTGAGCCTCATACC -3′ and 5′-
576 GCTTCAGAAAAAGAGAATACTCCT -3′ for *EXOC6A* KO-1(gRNA1) and 5′-
577 TTGGGTCAGTGATTTGAATTG -3′ and 5′- CCAAATAATCTGTAATTCCCATA -3′
578 for *EXOC6A* KO-2 (gRNA 2 and 3). The sequences of PCR products were then
579 confirmed as shown in Fig. S3A. Based on sequence analysis, a schematic diagram of
580 the predicted amino acid sequence is shown in Fig. S3B. Also, the protein expression
581 of expanded colonies was confirmed by Western blotting (Fig. S3C) and IF (Fig. S3E
582 and F).
583 RPE1-based doxycycline (DOX)-inducible cell lines were as described previously
584 (Wu et al., 2018). To obtain RPE1 cell lines that inducibly expressed GFP-EXOC6A,
585 GFP-Myo-Va-GTD, and mCherry-Myo-Va-GTD, lentiviruses generated using the
586 target cDNAs in the pLVX-tight-puro vector were used to infect RPE1 Tet-On cells
587 (stably expressing rtTA, Clontech). The infected cells were sterile-sorted using a cell
588 sorter (FACSAria, BD Biosciences) for GFP or mCherry, and the positive cells were
589 selected and expanded as inducible cell lines.
590 The siRNAs and non-targeting siRNA control were transfected into cells using
591 Lipofectamine RNAiMAX (Invitrogen), according to the manufacturer's protocol. To
592 increase knockdown efficiency, two rounds of silencing were used before the
593 experiments. To ensure the specificity of gene knockdown and minimize off-target
594 effects, we used siRNA sequences that have been validated in our previous studies (Wu
595 et al., 2018). The efficiency of gene depletion was confirmed by Western blotting. The
596 siRNA sequences for siEHD1 (5′- GGAGAGAUCUACCAGAAGA-3′), siGolgin-160
597 (5′-CAGCCUCCUUGGCCGCGAGGGCCUC-3′), and siARP2 (5′-
598 CCAGCUUUGGUUGGAAGACCUAUUA-3′) were purchased from Invitrogen.

599 **Immunoprecipitation and Western blotting**

600 RPE1 cells were lysed in RIPA buffer (50 mM Tris-HCl, pH 8.0, 150 mM NaCl, 1%
601 NP-40, 0.5% sodium deoxycholate, 20 mM β-glycerophosphate, 20 mM NaF, 1 mM
602 Na3VO4) supplemented with protease inhibitors (1 mg/mL leupeptin, 1 mg/mL
603 pepstatin, and 1 mg/mL aprotinin) for 1 h at 4°C. Lysates were clarified by
604 centrifugation for 10 min at 4°C, and the supernatants were immunoprecipitated with
605 the indicated antibodies for 2 h at 4°C. Protein G Sepharose beads were subsequently
606 added and incubated overnight at 4°C with gentle rotation. The beads were then washed
607 three times with RIPA buffer. Bound proteins were eluted by boiling in SDS sample
608 buffer, separated by SDS-PAGE, and analyzed by Western blotting with the appropriate
609 antibodies.

610 **Immunofluorescence confocal microscopy**

611 Immunofluorescence confocal microscopy was carried out as previously described
612 (Wu et al., 2018). Briefly, cells were grown on coverslips and fixed in methanol at
613 −20 °C for 20 min. The cells were then blocked with 10% normal goat serum in PBST.
614 After blocking, the cells were incubated with primary antibodies, washed with PBST,
615 and then incubated with Alexa Fluor 488-, 568-, or 647-conjugated secondary
616 antibodies (1/500; Invitrogen). The samples were visualized using an LSM880
617 Airyscan system (Carl Zeiss). FRAP experiments were performed on live RPE1 cells
618 co-expressing GFP-EXOC6A and mCherry-Myo-Va-GTD using a Zeiss LSM 880
619 confocal microscope. Time-lapse imaging was conducted with a time interval of 20
620 seconds. At each time point, Z-stacks consisting of 5 optical sections were captured to
621 cover the entire structure. Following the acquisition of 5 pre-bleach baseline images,
622 the GFP-EXOC6A and mCherry-Myo-Va-GTD signals within a defined region of
623 interest were photo-bleached using the 405 nm laser at 100% intensity for 100 iterations.
624 The fluorescence recovery was monitored over time, and intensity changes were
625 quantified from maximum intensity projections of the Z-stacks using ZEN software.
626

627 **Super-resolution microscopy (3D-SIM)**

628 The cells were fixed and stained as described (see above), and multi-colored beads
629 (100 nm; Invitrogen) were added before mounting. Sixteen-bit super-resolution images
630 with five phases and five rotations were obtained using a Zeiss ELYRA PS.1 LSM780
631 system or a Zeiss ELYRA7 system (Carl Zeiss). We used a plan-apochromatic 63×/1.4
632 NA oil-immersion M27 objective in combination with the default grid (stripe sim in
633 ELYRA PS.1 and Lattice sim plus SIM square). We used the "optimized" setting for
634 the z-stack interval. The raw images were reconstructed using ZEN Black (Carl Zeiss)
635 under the default parameters. The reconstructed images were corrected with signals of

636 beads for chromatic aberration in the *x*, *y*, and *z* directions, and the images were aligned
637 accordingly with ZEN Black. We followed the standard guidelines (Demmerle et al.,
638 2017) and used the SIM-Check software (Ball et al., 2015) to verify the raw,
639 reconstructed, and calibrated data. To visualize centriole and axoneme structures during
640 live-cell imaging, we employed SiR-tubulin, a fluorogenic probe that binds to
641 endogenous microtubules (spirochrome).

642 **Ultrastructure expansion microscopy (U-ExM)**

643 U-ExM was used to reveal the fine cellular architecture of the cells. Cells were
644 processed for this U-ExM as previously described (Gambarotto et al., 2019). In brief,
645 cells were fixed with methanol or 4% PFA based on our target. First, cells on coverslips
646 were incubated in a PBS solution containing 0.7% formaldehyde (FA; 36.5–38%;
647 F8775; Sigma-Aldrich) plus 0.15% acrylamide (AA; 40%; A4058; Sigma-Aldrich) for
648 5 h at 37 °C. Next, the cells on coverslips were incubated in U-ExM monomer solution,
649 composed of 19% (wt/wt) sodium acrylate (SA; 97–99%; 408220; Sigma-Aldrich),
650 10% (wt/wt) AA, and 0.1% (wt/wt) *N*,*N*′-methylenebisacrylamide (BIS; 2%; M1533;
651 Sigma-Aldrich) at 37 °C for 1 h in the dark for gelation. We transferred coverslips with
652 gel to 6-well plates, added 1 mL denaturing buffer (200 mM SDS, 200 mM NaCl, and
653 50 mM Tris in ultrapure water, pH 9), and shook for 15 min at room temperature (RT).
654 We then separated gel from coverslips and transferred the gel to 1.5 mL centrifuge tubes
655 with fresh denaturing buffer, then incubated at 95 °C for 30 min. After denaturation,
656 the gels were placed in beakers filled with ddH2O overnight for expansion. For
657 antibody staining, the gels were PBS washed and then incubated with primary
658 antibodies for 1 or 2 nights at RT (depending on the antibodies). The gels were washed
659 in PBST (PBS plus 0.1% tween20) and incubated with a secondary antibody for 3 h at
660 37 °C. The gels expanded by around 4x after this treatment. The samples were then
661 visualized using an LSM880 Airyscan system (Carl Zeiss).
662

663 **TEM and CLEM**

664 Cells were processed for transmission electron microscopy and CLEM as
665 previously described (Reddick and Alto, 2012). Briefly, RPE1 and RPE1-based
666 *EXOC6A* KO cells were grown on Aclar film (Electron Microscopy Sciences) and fixed
667 in 2% glutaraldehyde (GA) containing 1% tannic acid in 0.1 M cacodylate buffer. The
668 fixed cells were post-fixed with 1% OsO_4 in 0.1 M cacodylate buffer at room
669 temperature (RT) for 30 min. Then, the cells were further stained with 1% uranyl acetate
670 at RT for 1 h, dehydrated in a graded series of ethanol, infiltrated, and embedded in
671 Spurr's resin. Ultrathin sections (70 nm) were stained with 4% uranyl acetate (UA) and

672 Reynold's lead citrate for 10 min and examined with an electron microscope (Tecnai
673 G2 Spirit TWIN, FEI).
674 For CLEM, RPE1-based GFP-EXOC6A-inducible cells were grown on laser-
675 etched glass gridded coverslips affixed to the bottom of live-cell dishes (MatTek). Cells
676 were treated with DOX for 24 h and serum starved for 2 or 24 h. The cells were then
677 fixed with 2 % glutaraldehyde plus 1% tannic acid in 0.1 M cacodylate buffer, and the
678 GFP-EXOC6A signals were imaged via 3D-SIM using a Zeiss ELYRA system (Carl
679 Zeiss). The cells were then embedded in EPON resin. After EPON polymerization, resin
680 blocks were detached from the glass dishes. Using the grid patterns imprinted in the
681 resin, serial thin sections (70 nm) of the squares of interest were cut. The sections were
682 stained with 4% uranyl acetate and Reynold's lead citrate for 10 min, and the cells were
683 examined with an electron microscope (Tecnai G2 Spirit TWIN, FEI). All EM images
684 were processed using Gatan Digital Micrograph software (Gatan).

685 **Statistics and reproducibility**

686 Statistical analyses were performed using GraphPad Prism. Results are presented as
687 mean ± standard derivation (s.d.), as specified in the figure legends. Sample size and
688 the number of repeated experiments are also described in the legends. Statistical
689 differences between two datasets were analyzed using the two-tailed paired Student's *t*-
690 test. The precise *P*-values are shown in the figures. $P < 0.05$ was considered statistically
691 significant. All experiments were repeated at least three times.

692

693

Conflicts of interest

The authors declare no conflicts of interest.

Author contributions

Conceptualization: TLL and TKT; Investigation: TLL and CTW; Methodology: TLL, CTW, and TKT; Resource: TLL and TKT; Original Draft: TLL and TKT; Writing: TLL and TKT; Review & Editing: TLL, CTW, and TKT.

Acknowledgments

The authors acknowledge support from the Flow Cytometry Core Facility (IBMS, AS-CFII-111-212) for the cell-sorting service, the DNA Sequencing Core Facility (IBMS, AS-CFII-113-A12) for the DNA sequencing analysis, the Light Microscopy Core Facility (IBMS and IMB), and the EM core facilities (IMB and ICOB) of Academia Sinica. This work was supported by grants from Academia Sinica (AS-IA-109-L04) and the National Science and Technology Council, Taiwan (NSTC 112-2320-B-001-002; NSTC 112-2326-B-001-010) to TKT; and from the National Institutes of Health R01AI184984 to CTW.

References

Andreu-Cervera, A., M. Catala, and S. Schneider-Maunoury. 2021. Cilia, ciliopathies and hedgehog-related forebrain developmental disorders. *Neurobiol Dis*. 150:105236.

Ball, G., J. Demmerle, R. Kaufmann, I. Davis, I.M. Dobbie, and L. Schermelleh. 2015. SIMcheck: a Toolbox for Successful Super-resolution Structured Illumination Microscopy. *Sci Rep*. 5:15915.

Bowser, R., and P. Novick. 1991. Sec15 protein, an essential component of the exocytotic apparatus, is associated with the plasma membrane and with a soluble 19.5S particle. *The Journal of cell biology*. 112:1117-1131.

Breslow, D.K., and A.J. Holland. 2019. Mechanism and Regulation of Centriole and Cilium Biogenesis. *Annual review of biochemistry*. 88:691-724.

Cao, M., X. Zou, C. Li, Z. Lin, N. Wang, Z. Zou, Y. Ye, J. Seemann, B. Levine, Z. Tang, and Q. Zhong. 2023. An actin filament branching surveillance system regulates cell cycle progression, cytokinesis and primary ciliogenesis. *Nature Communications*. 14:1687.

Chiba, S., Y. Amagai, Y. Homma, M. Fukuda, and K. Mizuno. 2013. NDR2-mediated Rabin8 phosphorylation is crucial for ciliogenesis by switching binding

728 specificity from phosphatidylserine to Sec15. *The EMBO journal*. 32:874-885.
729 Coulter, M.E., D. Musaev, E.M. DeGennaro, X. Zhang, K. Henke, K.N. James, R.S. Smith,
730 R.S. Hill, J.N. Partlow, A.-S. Muna, A.S. Kamumbu, N. Hatem, A.J. Barkovich, J.
731 Aziza, N. Chassaing, M.S. Zaki, T. Sultan, L. Burglen, A. Rajab, L. Al-Gazali, G.H.
732 Mochida, M.P. Harris, J.G. Gleeson, and C.A. Walsh. 2020. Regulation of human
733 cerebral cortical development by EXOC7 and EXOC8, components of the
734 exocyst complex, and roles in neural progenitor cell proliferation and survival.
735 *Genetics in Medicine*. 22:1040-1050.
736 Dawe, H.R., H. Farr, and K. Gull. 2007. Centriole/basal body morphogenesis and
737 migration during ciliogenesis in animal cells. *Journal of cell science*. 120:7-15.
738 Demmerle, J., C. Innocent, A.J. North, G. Ball, M. Müller, E. Miron, A. Matsuda, I.M.
739 Dobbie, Y. Markaki, and L. Schermelleh. 2017. Strategic and practical guidelines
740 for successful structured illumination microscopy. *Nat Protoc*. 12:988-1010.
741 Dixon-Salazar, T.J., J.L. Silhavy, N. Udpa, J. Schroth, S. Bielas, A.E. Schaffer, J. Olvera, V.
742 Bafna, M.S. Zaki, G.H. Abdel-Salam, L.A. Mansour, L. Selim, S. Abdel-Hadi, N.
743 Marzouki, T. Ben-Omran, N.A. Al-Saana, F.M. Sonmez, F. Celep, M. Azam, K.J.
744 Hill, A. Collazo, A.G. Fenstermaker, G. Novarino, N. Akizu, K.V. Garimella, C.
745 Sougnez, C. Russ, S.B. Gabriel, and J.G. Gleeson. 2012. Exome sequencing can
746 improve diagnosis and alter patient management. *Sci Transl Med*. 4:138ra178.
747 Donovan, K.W., and A. Bretscher. 2012. Myosin-V is activated by binding secretory
748 cargo and released in coordination with Rab/exocyst function. *Dev Cell*. 23:769-
749 781.
750 Donovan, K.W., and A. Bretscher. 2015. Tracking individual secretory vesicles during
751 exocytosis reveals an ordered and regulated process. *The Journal of cell biology*.
752 210:181-189.
753 Feng, S., A. Knodler, J. Ren, J. Zhang, X. Zhang, Y. Hong, S. Huang, J. Peranen, and W.
754 Guo. 2012. A Rab8 guanine nucleotide exchange factor-effector interaction
755 network regulates primary ciliogenesis. *The Journal of biological chemistry*.
756 287:15602-15609.
757 Firestone, A.J., J.S. Weinger, M. Maldonado, K. Barlan, L.D. Langston, M. O'Donnell, V.I.
758 Gelfand, T.M. Kapoor, and J.K. Chen. 2012. Small-molecule inhibitors of the
759 AAA+ ATPase motor cytoplasmic dynein. *Nature*. 484:125-129.
760 Gambarotto, D., F.U. Zwettler, M. Le Guennec, M. Schmidt-Cernohorska, D. Fortun, S.
761 Borgers, J. Heine, J.-G. Schloetel, M. Reuss, M. Unser, E.S. Boyden, M. Sauer, V.
762 Hamel, and P. Guichard. 2019. Imaging cellular ultrastructures using expansion
763 microscopy (U-ExM). *Nature Methods*. 16:71-74.
764 Ganga, A.K., M.C. Kennedy, M.E. Oguchi, S. Gray, K.E. Oliver, T.A. Knight, E.M. De La
765 Cruz, Y. Homma, M. Fukuda, and D.K. Breslow. 2021. Rab34 GTPase mediates

766 ciliary membrane formation in the intracellular ciliogenesis pathway. *Curr Biol*.
767 31:2895-2905.e2897.
768 Garcia-Gonzalo, F.R., S.C. Phua, E.C. Roberson, G. Garcia, 3rd, M. Abedin, S. Schurmans,
769 T. Inoue, and J.F. Reiter. 2015. Phosphoinositides Regulate Ciliary Protein
770 Trafficking to Modulate Hedgehog Signaling. *Dev Cell*. 34:400-409.
771 Garcia-Gonzalo, F.R., and J.F. Reiter. 2017. Open Sesame: How Transition Fibers and the
772 Transition Zone Control Ciliary Composition. *Cold Spring Harb Perspect Biol*. 9.
773 Ghossoub, R., A. Molla-Herman, P. Bastin, and A. Benmerah. 2011. The ciliary pocket:
774 a once-forgotten membrane domain at the base of cilia. *Biology of the cell*.
775 103:131-144.
776 Gonçalves, J., and L. Pelletier. 2017. The Ciliary Transition Zone: Finding the Pieces and
777 Assembling the Gate. *Mol Cells*. 40:243-253.
778 Graser, S., Y.D. Stierhof, S.B. Lavoie, O.S. Gassner, S. Lamla, M. Le Clech, and E.A. Nigg.
779 2007. Cep164, a novel centriole appendage protein required for primary cilium
780 formation. *The Journal of cell biology*. 179:321-330.
781 Guo, J., H. Higginbotham, J. Li, J. Nichols, J. Hirt, V. Ghukasyan, and E.S. Anton. 2015.
782 Developmental disruptions underlying brain abnormalities in ciliopathies. *Nat*
783 *Commun*. 6:7857.
784 Jensen, V.L., and M.R. Leroux. 2017. Gates for soluble and membrane proteins, and
785 two trafficking systems (IFT and LIFT), establish a dynamic ciliary signaling
786 compartment. *Curr Opin Cell Biol*. 47:83-91.
787 Jin, Y., A. Sultana, P. Gandhi, E. Franklin, S. Hamamoto, A.R. Khan, M. Munson, R.
788 Schekman, and L.S. Weisman. 2011. Myosin V transports secretory vesicles via
789 a Rab GTPase cascade and interaction with the exocyst complex. *Dev Cell*.
790 21:1156-1170.
791 Kee, H.L., J.F. Dishinger, T.L. Blasius, C.J. Liu, B. Margolis, and K.J. Verhey. 2012. A size-
792 exclusion permeability barrier and nucleoporins characterize a ciliary pore
793 complex that regulates transport into cilia. *Nat Cell Biol*. 14:431-437.
794 Kim, J., H. Jo, H. Hong, M.H. Kim, J.M. Kim, J.K. Lee, W.D. Heo, and J. Kim. 2015. Actin
795 remodelling factors control ciliogenesis by regulating YAP/TAZ activity and
796 vesicle trafficking. *Nat Commun*. 6:6781.
797 Kim, J., J.E. Lee, S. Heynen-Genel, E. Suyama, K. Ono, K. Lee, T. Ideker, P. Aza-Blanc, and
798 J.G. Gleeson. 2010. Functional genomic screen for modulators of ciliogenesis
799 and cilium length. *Nature*. 464:1048-1051.
800 Knödler, A., S. Feng, J. Zhang, X. Zhang, A. Das, J. Peränen, and W. Guo. 2010.
801 Coordination of Rab8 and Rab11 in primary ciliogenesis. *Proc Natl Acad Sci U S*
802 *A*. 107:6346-6351.
803 Lin, Y.N., C.T. Wu, Y.C. Lin, W.B. Hsu, C.J. Tang, C.W. Chang, and T.K. Tang. 2013. CEP120

804 interacts with CPAP and positively regulates centriole elongation. *J Cell Biol*.
805 202:211-219.
806 Long, H., and K. Huang. 2019. Transport of Ciliary Membrane Proteins. *Front Cell Dev*
807 *Biol*. 7:381.
808 Lu, Q., C. Insinna, C. Ott, J. Stauffer, P.A. Pintado, J. Rahajeng, U. Baxa, V. Walia, A.
809 Cuenca, Y.S. Hwang, I.O. Daar, S. Lopes, J. Lippincott-Schwartz, P.K. Jackson, S.
810 Caplan, and C.J. Westlake. 2015. Early steps in primary cilium assembly require
811 EHD1/EHD3-dependent ciliary vesicle formation. *Nat Cell Biol*. 17:228-240.
812 Martin-Urdiroz, M., M.J. Deeks, C.G. Horton, H.R. Dawe, and I. Jourdain. 2016. The
813 Exocyst Complex in Health and Disease. *Frontiers in Cell and Developmental*
814 *Biology*. 4.
815 Mei, K., and W. Guo. 2018. The exocyst complex. *Current Biology*. 28:R922-R925.
816 Meire, F., I. Delpierre, C. Brachet, F. Roulez, C. Van Nechel, F. Depasse, C. Christophe,
817 B. Menten, and E. De Baere. 2011. Nonsyndromic bilateral and unilateral optic
818 nerve aplasia: first familial occurrence and potential implication of CYP26A1
819 and CYP26C1 genes. *Mol Vis*. 17:2072-2079.
820 Mukhopadhyay, S., X. Wen, N. Ratti, A. Loktev, L. Rangell, S.J. Scales, and P.K. Jackson.
821 2013. The ciliary G-protein-coupled receptor Gpr161 negatively regulates the
822 Sonic hedgehog pathway via cAMP signaling. *Cell*. 152:210-223.
823 Nachury, M.V., A.V. Loktev, Q. Zhang, C.J. Westlake, J. Peranen, A. Merdes, D.C. Slusarski,
824 R.H. Scheller, J.F. Bazan, V.C. Sheffield, and P.K. Jackson. 2007. A core complex
825 of BBS proteins cooperates with the GTPase Rab8 to promote ciliary membrane
826 biogenesis. *Cell*. 129:1201-1213.
827 Nachury, M.V., E.S. Seeley, and H. Jin. 2010. Trafficking to the ciliary membrane: how
828 to get across the periciliary diffusion barrier? *Annu Rev Cell Dev Biol*. 26:59-87.
829 Nigg, E.A., and J.W. Raff. 2009. Centrioles, centrosomes, and cilia in health and disease.
830 *Cell*. 139:663-678.
831 Palmer, K.J., H. Hughes, and D.J. Stephens. 2009. Specificity of cytoplasmic dynein
832 subunits in discrete membrane-trafficking steps. *Mol Biol Cell*. 20:2885-2899.
833 Ran, F.A., P.D. Hsu, J. Wright, V. Agarwala, D.A. Scott, and F. Zhang. 2013. Genome
834 engineering using the CRISPR-Cas9 system. *Nat Protoc*. 8:2281-2308.
835 Reddick, L.E., and N.M. Alto. 2012. Correlative light and electron microscopy (CLEM)
836 as a tool to visualize microinjected molecules and their eukaryotic sub-cellular
837 targets. *J Vis Exp*:e3650.
838 Rivera-Molina, F.E., Z. Xi, E. Reales, B. Wang, and D. Toomre. 2021. Exocyst complex
839 mediates recycling of internal cilia. *Current Biology*. 31:5580-5589.e5585.
840 Sattar, S., and J.G. Gleeson. 2011. The ciliopathies in neuronal development: a clinical
841 approach to investigation of Joubert syndrome and Joubert syndrome-related

842 disorders. *Developmental medicine and child neurology*. 53:793-798.
843 Schmidt, K.N., S. Kuhns, A. Neuner, B. Hub, H. Zentgraf, and G. Pereira. 2012. Cep164
844 mediates vesicular docking to the mother centriole during early steps of
845 ciliogenesis. *The Journal of cell biology*. 199:1083-1101.
846 Seixas, C., S.Y. Choi, N. Polgar, N.L. Umberger, M.P. East, X. Zuo, H. Moreiras, R.
847 Ghossoub, A. Benmerah, R.A. Kahn, B. Fogelgren, T. Caspary, J.H. Lipschutz, and
848 D.C. Barral. 2016. Arl13b and the exocyst interact synergistically in ciliogenesis.
849 *Mol Biol Cell*. 27:308-320.
850 Shaheen, R., E. Faqeih, M.J. Alshammari, A. Swaid, L. Al-Gazali, E. Mardawi, S. Ansari,
851 S. Sogaty, M.Z. Seidahmed, M.I. AlMotairi, C. Farra, W. Kurdi, S. Al-Rasheed, and
852 F.S. Alkuraya. 2013. Genomic analysis of Meckel–Gruber syndrome in Arabs
853 reveals marked genetic heterogeneity and novel candidate genes. *European*
854 *Journal of Human Genetics*. 21:762-768.
855 Spektor, A., W.Y. Tsang, D. Khoo, and B.D. Dynlacht. 2007. Cep97 and CP110 suppress a
856 cilia assembly program. *Cell*. 130:678-690.
857 Stuck, M.W., W.M. Chong, J.C. Liao, and G.J. Pazour. 2021. Rab34 is necessary for early
858 stages of intracellular ciliogenesis. *Curr Biol*. 31:2887-2894.e2884.
859 TerBush, D.R., T. Maurice, D. Roth, and P. Novick. 1996. The Exocyst is a multiprotein
860 complex required for exocytosis in Saccharomyces cerevisiae. *The EMBO*
861 *journal*. 15:6483-6494.
862 TerBush, D.R., and P. Novick. 1995. Sec6, Sec8, and Sec15 are components of a
863 multisubunit complex which localizes to small bud tips in Saccharomyces
864 cerevisiae. *The Journal of cell biology*. 130:299-312.
865 Tsai, J.-J., W.-B. Hsu, J.-H. Liu, C.-W. Chang, and T.K. Tang. 2019. CEP120 interacts with
866 C2CD3 and Talpid3 and is required for centriole appendage assembly and
867 ciliogenesis. *Scientific Reports*. 9:6037.
868 Turkyilmaz, A., E. Kurnaz, and A. Cayir. 2021. First Report of a de novo 10q23.31q23.33
869 Microdeletion: Obesity, Intellectual Disability and Microcephaly. *Mol*
870 *Syndromol*. 12:258-262.
871 Valente, E.M., R.O. Rosti, E. Gibbs, and J.G. Gleeson. 2014. Primary cilia in
872 neurodevelopmental disorders. *Nature reviews. Neurology*. 10:27-36.
873 Van Bergen, N.J., S.M. Ahmed, F. Collins, M. Cowley, A. Vetro, R.C. Dale, D.H. Hock, C.
874 de Caestecker, M. Menezes, S. Massey, G. Ho, T. Pisano, S. Glover, J. Gusman,
875 D.A. Stroud, M. Dinger, R. Guerrini, I.G. Macara, and J. Christodoulou. 2020.
876 Mutations in the exocyst component EXOC2 cause severe defects in human
877 brain development. *J Exp Med*. 217.
878 Westlake, C.J., L.M. Baye, M.V. Nachury, K.J. Wright, K.E. Ervin, L. Phu, C. Chalouni, J.S.
879 Beck, D.S. Kirkpatrick, D.C. Slusarski, V.C. Sheffield, R.H. Scheller, and P.K.

880 Jackson. 2011. Primary cilia membrane assembly is initiated by Rab11 and
881 transport protein particle II (TRAPPII) complex-dependent trafficking of Rabin8
882 to the centrosome. *Proc Natl Acad Sci U S A*. 108:2759-2764.
883 Wingfield, J.L., K.F. Lechtreck, and E. Lorentzen. 2018. Trafficking of ciliary membrane
884 proteins by the intraflagellar transport/BBSome machinery. *Essays Biochem*.
885 62:753-763.
886 Wu, B., and W. Guo. 2015. The Exocyst at a Glance. *Journal of cell science*. 128:2957-
887 2964.
888 Wu, C.T., H.Y. Chen, and T.K. Tang. 2018. Myosin-Va is required for preciliary vesicle
889 transportation to the mother centriole during ciliogenesis. *Nat Cell Biol*.
890 20:175-185.
891 Xu, S., Y. Liu, Q. Meng, and B. Wang. 2018. Rab34 small GTPase is required for
892 Hedgehog signaling and an early step of ciliary vesicle formation in mouse.
893 *Journal of cell science*. 131.
894 Yadav, S., M.A. Puthenveedu, and A.D. Linstedt. 2012. Golgin160 recruits the dynein
895 motor to position the Golgi apparatus. *Dev Cell*. 23:153-165.
896 Yoshimura, S., J. Egerer, E. Fuchs, A.K. Haas, and F.A. Barr. 2007. Functional dissection
897 of Rab GTPases involved in primary cilium formation. *The Journal of cell biology*.
898 178:363-369.
899 Zuo, X., W. Guo, and J.H. Lipschutz. 2009. The exocyst protein Sec10 is necessary for
900 primary ciliogenesis and cystogenesis in vitro. *Mol Biol Cell*. 20:2522-2529.
901 Zuo, X., G. Lobo, D. Fulmer, L. Guo, Y. Dang, Y. Su, D.V. Ilatovskaya, D. Nihalani, B. Rohrer,
902 S.C. Body, R.A. Norris, and J.H. Lipschutz. 2019. The exocyst acting through the
903 primary cilium is necessary for renal ciliogenesis, cystogenesis, and
904 tubulogenesis. *The Journal of biological chemistry*. 294:6710-6718.
905
906
907

908 ## Figure Legends

909 **Figure 1. Colocalization patterns of EXOC6A and myosin-Va at preciliary vesicles,**
910 **ciliary vesicles, and ciliary sheath during ciliogenesis.**

911 (A) RPE1-based mCherry-Myo-Va-GTD cells were treated with Dox for 24 h, followed
912 by serum starvation for 2h. Cells were then stained with antibodies against EXOC6A
913 (green) and polyglutamylated tubulin (Glu-tub) (gray) and analyzed using
914 immunofluorescence confocal microscopy. (B and C) RPE1-based mCherry-Myo-Va-
915 GTD-inducible cells were treated as described in A and immunostained with antibodies
916 against EXOC6A (green), CEP120 (centriole marker), and CEP164 (distal appendage
917 marker, gray). Images were captured using 3D-SIM or ultra-expansion microscopy (U-
918 ExM) with an LSM880 confocal system. (D) CLEM analysis of the localization of
919 GFP-EXOC6A during ciliogenesis. RPE1-based GFP-EXOC6A-inducible cells were
920 treated with Dox for 24 h and subjected to serum starvation for 2 or 24 h to observe the
921 CVs or cilia membrane, respectively. Images were taken via SIM and TEM and then
922 merged based on their relative localization. GFP-EXOC6A signals were located at
923 PCVs, CVs (i-ii), and the ciliary membrane (iii-iv). (E) RPE1-based GFP-EXOC6A
924 and mCherry-Myo-Va-GTD-inducible cells were treated with Dox for 24 h and
925 analyzed via 3D-SIM using the indicated antibodies. Right panels show fluorescence
926 profile plots. EXOC6A colocalized with myosin-Va at the ciliary sheath, while
927 ARL13B (i) and INPP5E (iii) are the ciliary shaft markers. Scale bars are 1 μm.
928

929 **Figure 2. Spatial–temporal localization of EXOC6A and Myo-Va during**
930 **ciliogenesis.**

931 (A) RPE1-based mCherry-Myo-Va-GTD-inducible cells were treated with Dox for 24
932 h, serum starved, released at different time points, and analyzed via 3D-SIM using the
933 indicated antibodies. The white arrow indicates a tubule extending from the ciliary
934 membrane. (B, C) Schematic model showing the localization patterns of EXOC6A
935 (green) and Myo-Va (red) during ciliogenesis, and the percentages of cells with
936 different types of staining patterns (%) are shown in C. Scale bars are 1 μm.
937

938 **Figure 3. FRAP analysis of Myo-Va- and EXOC6A-labeled vesicles during**
939 **ciliogenesis.**

940 (A and B) RPE1-based GFP-EXOC6A and mCherry-Myo-Va-GTD-inducible cells
941 were treated with Dox for 24 h and serum starved for 30 min. Regions of CVs (A) or

942 the ciliary membrane (B) of the cells were photobleached using the LSM880 confocal
943 microscope with the 405 nm laser (related to Movies 1 and 2). Signal intensity of
944 EXOC6A is shown in the right panel. (C and D) Dynamic localization of GFP-
945 EXOC6A at CVs (C) or the ciliary membrane (D) during ciliogenesis. RPE1-based
946 GFP-EXOC6A-inducible cells were treated with Dox for 24 h and serum starved for 30
947 min. Images were taken using an Elyra 7 high-speed live-cell imaging system. Series
948 of images in (C) shows the progression of fusion of GFP-EXOC6A-associated vesicles
949 into CVs (white arrow). Series of images in (D) shows the process by which GFP-
950 EXOC6A-associated vesicles fuse into the ciliary pocket (white arrow) and
951 simultaneously exit or reintegrate into the ciliary pocket (red arrow). Some images also
952 show the release of tubule-like structures in the ciliary membrane (yellow arrow), or
953 the excretion of vesicles in the ciliary membrane (orange arrow). These data suggested
954 that the components of CVs, the ciliary pocket, and the ciliary membrane are highly
955 dynamic (related to Movies 4 and 5). Scale bars are 2 μm.
956

957 **Figure 4. Myo-Va and EHD1 are required for EXOC6A-labeled CV formation,**
958 **and EXOC6A is associated with Myo-Va.**

959 (A) Myo-Va is required for EXOC6A-labeled CV formation. RPE1-based *Myo-Va* KO
960 cells and WT cells immunostained with antibodies against EXOC6A (green) and Glu-
961 tub (red). Quantification of cells with EXOC6A-positive CVs (middle panel) and
962 immunoblotting results (right panel) are shown. (B) EXOC6A is not required for Myo-
963 Va-labeled CV formation. RPE1-based mCherry-Myo-Va-GTD-inducible cells against
964 *EXOC6A* KO background and WT cells were immunostained with antibodies against
965 Glu-tub (red). For easy differentiation, the mCherry-Myo-Va-GTD signal is converted
966 to green. Quantification of cells with Myo-Va-associated CVs (middle panel) and
967 immunoblotting results (right panel) are shown. (C) EHD1 is required for EXOC6A-
968 labeled CV formation. RPE1 cells treated with siControl or siEHD1 for 48 h were
969 immunostained with antibodies against EXOC6A (green) and Glu-tub (red).
970 Quantification of cells with EXOC6A-positive CVs (middle panel) and
971 immunoblotting results (right panel) are shown. (D) EXOC6A is not required for
972 EHD1-labeled CV formation. RPE1-based *EXOC6A* KO and WT cells were
973 immunostained with antibodies against EHD1 (green) and Glu-tub (red). Quantification
974 of cells with EHD1-positive CVS is shown (right panel). (E) Co-IP experiments
975 analyzed the association between EXOC6A and its potential binding proteins. Cell
976 lysates were immunoprecipitated (IP) with EXOC6A or Myo-Va antibodies, followed
977 by immunoblotting with the indicated antibodies. Error bars in A–D represent mean ±
978 s.d. from at least 3 independent experiments with 100 cells per experiment. *P*-value was

979 determined with two-tailed Student's *t*-test. $P < 0.05$ was considered statistically
980 significant. NS, not significant. Scale bars are 1 μm.
981

982 **Figure 5. Transportation of EXOC6A-associated vesicles to the mother-centriole**
983 **occurs via a dynein-, actin-, and MT-dependent pathway**

984 (A) Schematic showing the protocols of siRNA (left) or drug (right) treatment. (B)
985 RPE1 cells were treated with siControl or siGolgin160 and analyzed via confocal
986 fluorescence microscopy or immunoblotting using the indicated antibodies. (C) RPE1
987 cells were treated with 10 μM ciliobrevin D (i) or 10 μM nocodazole (ii) and analyzed
988 via confocal fluorescence microscopy using the indicated antibodies. (D-F) Cells with
989 EXOC6A-associated CVs (D), a positioned Golgi (E), or a cilia ratio (F) were analyzed
990 via 3D-SIM and quantified. Cells with a positioned Golgi were defined as those
991 showing all GM130-labeled Golgi signals concentrated within a 7 μm radius
992 surrounding the Glu-tub-labeled centrioles. (G) RPE1-based mCherry-myosin-Va-
993 GTD-inducible cells were treated with siARP2 as described in A (left) and analyzed via
994 confocal microscopy or immunoblotting using the indicated antibodies. (H, I)
995 Quantifications of the cilia ratio (H) and EXOC6A-associated CVs (I) is shown. (J)
996 RPE1 cells were treated with 200 μM CK666 or high-dose (10 μM) CytoD as described
997 in A (right panel) and analyzed via confocal microscopy using the indicated antibodies.
998 Quantification of the cilia ratio (H) and EXOC6A-associated CVs (I) is shown. * in (B,
999 right panel) indicates non-specific bands. Error bars represent mean ± s.d. from at least
1000 3 independent experiments with 100 randomly selected cells. *P*-value was determined
1001 with two-tailed Student's *t*-test. $P < 0.05$ was considered statistically significant. NS,
1002 not significant. Scale bars are 1 μm.

1003 **Figure 6. Loss of EXOC6A inhibits ciliogenesis, and some cells exhibit an**
1004 **abnormal ciliary morphology when passing through the CV block.**

1005 (A-C) RPE1-based mCherry-Myo-Va-GTD-inducible WT (A and B) and *EXOC6A*
1006 KO (A'and B') cells were treated with Dox for 24 h, serum starved (SS) at different
1007 time points, and analyzed via confocal fluorescence microscopy with the indicated
1008 antibodies. mCherry-Myo-Va-GTD signal is artificially converted to green for
1009 discrimination. (B) RPE1 WT and *EXOC6A* KO cells were serum starved at different
1010 time points and analyzed via confocal fluorescence microscopy with the indicated
1011 antibodies. For comparison, the intensities of ARBL13B and Glu-tub of *EXOC6A* KO
1012 cells with non-enhanced and enhanced signals are shown in B'. (C) Cilia ratio measured
1013 through ARL13B labeling (non-enhanced signal). (D and E) Quantitation of non-
1014 enhanced ARL13B (D) and non-enhanced Glu-tub intensity on cilia (E) of WT or

1015 *EXOC6A* KO cells is shown. (F) WT and *EXOC6A* KO cells were serum starved for 72
1016 h. Morphologies of normal or abnormal cilia, including DA, CVs, and ciliary
1017 membranes, were examined via EM (F) and quantified (G; N is the number of cells
1018 examined). Error bars in C, D, and E represent mean ± s.d. from at least 3 independent
1019 experiments from 100 randomly selected cells. *P*-value was determined with two-tailed
1020 Student's *t*-test. $P < 0.05$ was considered statistically significant. NS, not significant.
1021 Scale bars are 1 μm in A and B. Scale bars are 500 nm in F.
1022

1023 **Figure 7. EXOC6A is required for the recruitment of a subset of TZ proteins and**
1024 **ciliary membrane proteins to the cilia**

1025 (A) WT and *EXOC6A* KO cells were fixed for 2 h (A) or 24 h (B, C) after serum
1026 starvation and analyzed via confocal fluorescence microscopy using indicated
1027 antibodies. Glu-tub staining labeled the centriole. Quantification of the fluorescence
1028 signals of various MKS proteins, NPHP8, and ciliary membrane proteins (GRP161 and
1029 BBS9) is shown in the right panel. Error bars represent the mean ± s.d. from at least 3
1030 independent experiments with 100 randomly selected cells per experiment. *P*-value was
1031 determined with two-tailed Student's *t*-test. $P < 0.05$ was considered statistically
1032 significant. NS, not significant. Scale bars, 1 μm.
1033

1034 **Figure 8. Ciliogenesis model and comparison between WT and *EXOC6A* KO cells.**

1035 EXOC6A is located at the PCV/CV/ciliary sheath, and Myo-Va mediated the
1036 transportation of EXOC6A vesicles to the mother centriole via a dynein-, microtubule-,
1037 and actin-dependent pathway. EXOC6A-associated vesicles are continuously recruited
1038 and fused or excreted from the CVs or ciliary membrane. Depletion of EXOC6A
1039 impairs ciliogenesis, and most cells are arrested at the CV stage. There is a lack of MKS
1040 module proteins of the TZ in cilia with defects in *EXOC6A* KO cells. PCV, preciliary
1041 vesicle; CV, ciliary vesicle; DA, distal appendage; sDA, subdistal appendage.
1042

1043 **Supplementary Figure 1. Correlation of spatial localization of EXOC6A and Myo-**
1044 **Va during the early stages of ciliogenesis.**

1045 (A) RPE1-based mCherry-Myo-Va-GTD-inducible cells were treated with DOX for 24
1046 h and serum starved for 0, 15, and 30 min. Fluorescence intensities of EXOC6A (green)
1047 or Myo-Va-GTD (red) signals within a 2 μm radius surrounding the Glu-tub-labeled
1048 centrioles (white) were quantified and are shown in B (EXOC6A) and C (Myo-Va-
1049 GTD). Correlation R (Pearson correlation coefficient) between EXOC6A and Myo-Va
1050 is shown in D. Correlation R was analyzed using Zeiss Zen blue software. Error bars in

1051 B–D represent mean ± s.d. from at least 3 independent experiments with 100 randomly
1052 selected cells. P-value was determined with one-way ANOVA. $P < 0.05$ was considered
1053 statistically significant. NS, not significant. Scale bars are 1 μm.
1054

1055 **Supplementary Figure 2. Live-cell imaging of GFP-EXOC6A co-localized with**
1056 **Myo-Va-GTD at the ciliary membrane**

1057 (A) RPE1-based inducible cells expressing GFP-EXOC6A and mCherry-MyoVa-GTD
1058 were treated with Dox for 24 h, serum starved for 30 min, and SiR-tubulin was added
1059 to label centriole and axoneme. (B) Single channel image (green box in A) captured at
1060 the starting time point (0 sec). (C) Single channel image (red box in A) captured at
1061 frame 21 (197.577 sec). Scale bars are 1 μm.
1062

1063 **Supplementary Figure 3. Construction and Characterization of EXOC6A**
1064 **Knockout Cell Lines**

1065 (A) Schematic illustration of the CRISPR-Cas9 gene-editing strategies used to
1066 construct *EXOC6A*-KO RPE1 cells. (a) Construction of the KO-1 clone: using a single
1067 sgRNA1 targeting exon 2 of the EXOC6A gene. Gene sequence analysis confirms a 2
1068 bp deletion (del), resulting in a frameshift mutation. (b) Construction of the KO-2 clone:
1069 using a dual-sgRNA strategy (sgRNA 2 targeting exon 3 and sgRNA 3 targeting exon
1070 4). Gene sequence analysis confirms a large 204 bp deletion spanning the intron
1071 between exon 3 and 4 (including 88 bp at the intron). (B) Schematic diagram of the
1072 predicted protein products. Frameshift mutations in KO-1 and KO-2 were expected to
1073 lead to premature termination compared to the full-length Wild-Type (WT) protein (804
1074 aa), resulting in truncated non-functional peptides of 61 aa and 104 aa, respectively.
1075 (C) Immunoblot validation of knockout efficiency. Western blot analysis showed
1076 complete lossof EXOC6A protein in both KO-1 and KO-2 clones compared to WT
1077 RPE1 cells. (D) Quantitative analysis of cilia ratio in WT and *EXOC6A* KO clones. WT
1078 and KO Cells were treated with serum starvation for 24 h. Ciliary structures were
1079 visualized by ARL13B staining and categorized as cilia (blue), dot (yellow), or no
1080 structure (Non, red). Notably, both independent KO clones exhibited similar
1081 phenotypes, predominantly arresting at the "Dot" stage. Error bars represent the mean
1082 ± s.d. from three independent experiments (n=100 cells per experiment). (E and F)
1083 Immunofluorescence assays confirmed antibody specificity and the absence of protein
1084 expression in *EXOC6A* knockout clones. Wild-type cells and two independent *EXOC6A*
1085 knockout clones (KO-1 and KO-2) were serum-starved for 2h (E, for the CV phase) or
1086 24 h (F, for the ciliary phase) to induce ciliogenesis. WT cells showed clear EXOC6A

1087 localization at the CV or ciliary sheath, while no specific green signal was detected in
1088 either KO clone.

1089 **Supplementary Figure 4. *EXOC6A* deletion does not interfere with the removal of**
1090 **CP110 from the mother centriole.**

1091 WT and *EXOC6A* KO cells were fixed 24 h after serum starvation and analyzed via
1092 fluorescence confocal microscopy using the indicated antibodies. (B) Percentages of
1093 cells with one or two CP110 dots are shown. Error bars represent the mean ± s.d. from
1094 at least 3 independent experiments with 100 cells per experiment. *P*-value was
1095 determined with two-tailed Student's *t*-test. NS, not significant. Scale bars are 1 μm.
1096

1097 **Supplementary Figure 5. Low doses of Cytochalasin D (CytoD) promote cilia**
1098 **elongation, whereas higher concentrations (greater than 4 μM) inhibit ciliogenesis.**

1099 (A) RPE1 cells were treated with different concentrations of Cytochalasin D (CytoD),
1100 including control (0.1% DMSO), 200 nM, 1 μM, 2 μM, 4 μM, 7 μM, and 10 μM.
1101 Quantification of ciliary length labeled with ARL13B antibody (B) and cilia ratio (C)
1102 are shown. P-values were determined with a two-tailed Student's *t*-test. $P < 0.05$ was
1103 considered statistically significant. Error bars represent the mean ± s.d. of 100 randomly
1104 selected cells from at least 3 independent experiments. Scale bars are 2 μm.

1105 **Supplementary Figure 6. Rescue of ciliogenesis defects in EXOC6A knockout cells**
1106 **by GFP-EXOC6A re-expression.**

1107 **(A)** Representative immunofluorescence images of RPE1 cells (WT, WT+GFP-
1108 EXOC6A, *EXOC6A* KO, and *EXOC6A* KO+GFP-EXOC6A) stained for ARL13B (red)
1109 and Glu-tubulin (white). **(B)** Quantitative analysis of ARL13B-labeled cilia phenotypes.
1110 Data are presented as the mean ± s.d. of 100 randomly selected cells from at least three
1111 independent experiments. *P*-value was determined with two-tailed Student's *t*-test. $P <$
1112 0.05 was considered statistically significant. NS, not significant. Scale bars are 1 μm.
1113
1114
1115
1116

1117 **Source Data. Uncropped images of Western blots shown in the main figures.**
1118

1119 **Supplementary Video**

1120 Supplementary Video 1 Related to Fig. 3A. RPE1-based inducible cells expressing
1121 GFP-EXOC6A and mCherry-Myo-Va-GTD were treated with Dox for 24 h and then

1122 serum starved for 30 min. Live cell images were taken using an LSM880 Carl Zeiss
1123 confocal system under a controlled CO2 (5%) and temperature (37 °C). Photobleaching
1124 was performed on the CVs. The first time point of photobleaching the CVs was at 2
1125 min, following which the CVs gradually recovered.
1126
1127 Supplementary Video 2 Related to Fig. 3B. RPE1-based inducible cells expressing
1128 GFP-EXOC6A and mCherry-Myo-Va-GTD were treated with Dox for 24 h and then
1129 serum starved for 30 min. Live cell images were taken using an LSM880 Carl Zeiss
1130 confocal system under a controlled CO2 (5%) and temperature (37 °C). Photobleaching
1131 was performed on the ciliary membrane. The first photobleaching time point for the
1132 ciliary membrane was at 2 min, after which the ciliary membrane gradually recovered.
1133
1134 Supplementary Video 3 Related to Fig. S2. RPE1-based inducible cells expressing
1135 GFP-EXOC6A and mCherry-MyoVa-GTD were treated with Dox for 24 h, then serum
1136 starved for 30 min, and SiR-tubulin was added to label centriole and axoneme. Live
1137 cell images were acquired using an Elyra 7 SIM Carl Zeiss confocal system under a
1138 controlled CO2 (5%) and temperature (37 °C).
1139
1140 Supplementary Video 4 Related to Fig. 3C. RPE1-based inducible cells expressing
1141 GFP-EXOC6A were treated with Dox for 24 h and then serum starved for 30 min. Live
1142 cell images were taken using an Elyra 7 SIM Carl Zeiss confocal system under a
1143 controlled CO2 (5%) and temperature (37 °C).
1144
1145 Supplementary Video 5 Related to Fig. 3D. RPE1-based inducible cells expressing
1146 GFP-EXOC6A were treated with Dox for 24 h and then serum starved for 30 min. Live
1147 cell images were taken using an Elyra 7 SIM Carl Zeiss confocal system under a
1148 controlled CO2 (5%) and temperature (37 °C).
1149
1150

Figure. 1

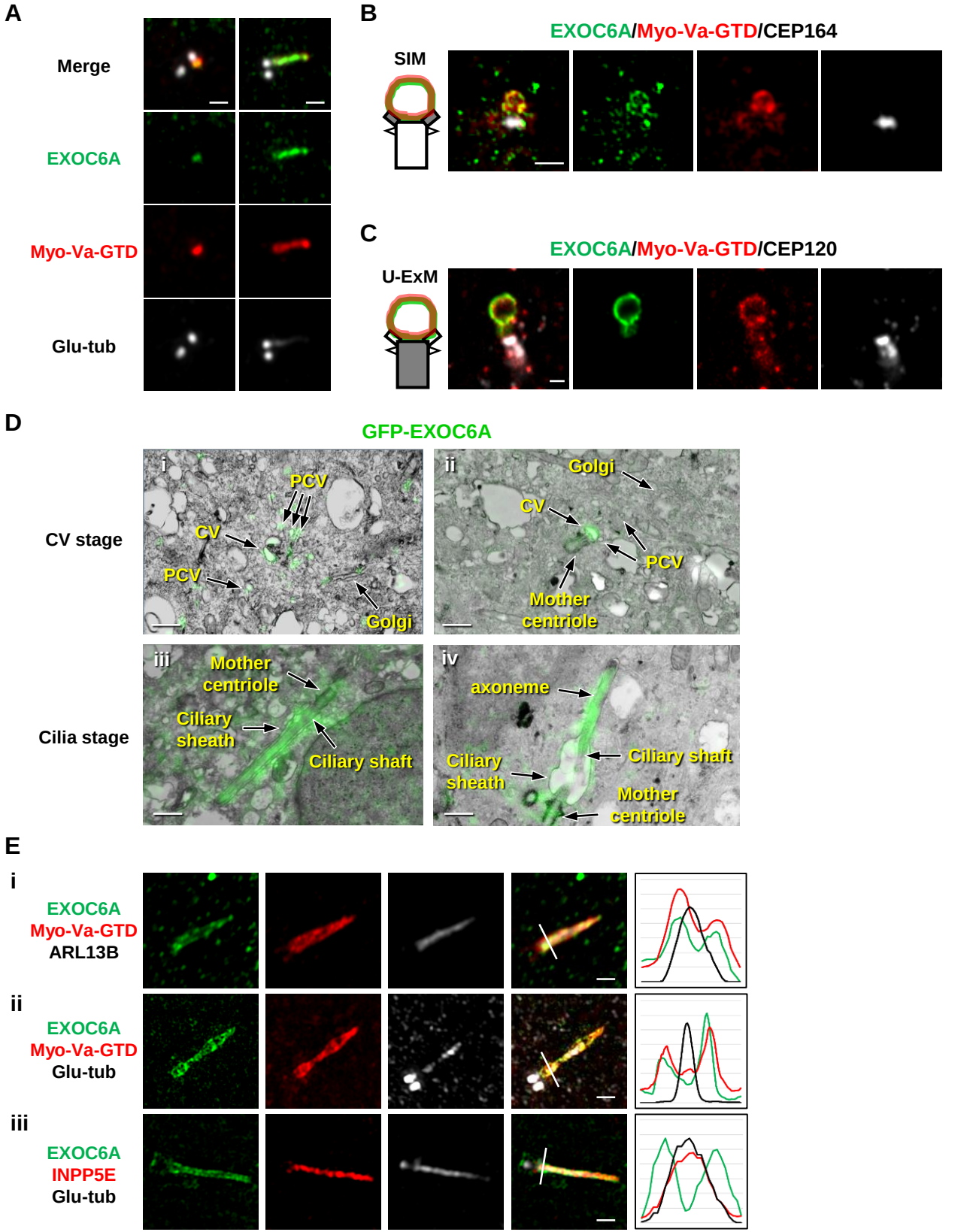
A
Merge
EXOC6A
Myo-Va-GTD
Glu-tub
B
EXOC6A/Myo-Va-GTD/CEP164
SIM
C
EXOC6A/Myo-Va-GTD/CEP120
U-ExM
D
GFP-EXOC6A
CV stage
i
PCV
CV
PCV
Golgi
ii
Golgi
CV
PCV
Mother centriole
Cilia stage
iii
Mother centriole
Ciliary sheath
Ciliary shaft
iv
axoneme
Ciliary sheath
Ciliary shaft
Mother centriole
E
i
EXOC6A
Myo-Va-GTD
ARL13B
ii
EXOC6A
Myo-Va-GTD
Glu-tub
iii
EXOC6A
INPP5E
Glu-tub

Figure. 2

A

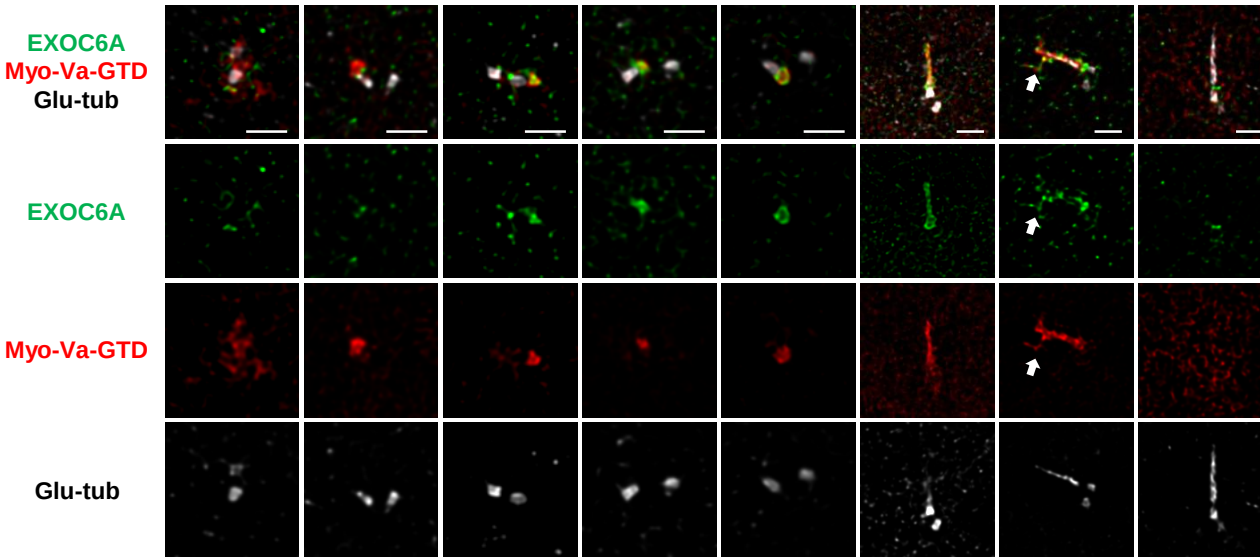

0min	15min	30min	45min	1h	2h	4h	24h
Type 1	Type 2	Type 3			Type 4		Type 5
		EXOC6A^{+}/Va^{+} at CV			EXOC6A^{+}/Va^{+} Elongated cilia		EXOC6A^{-}/Va^{-} Elongated cilia

B

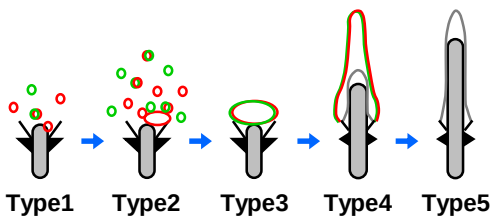

C

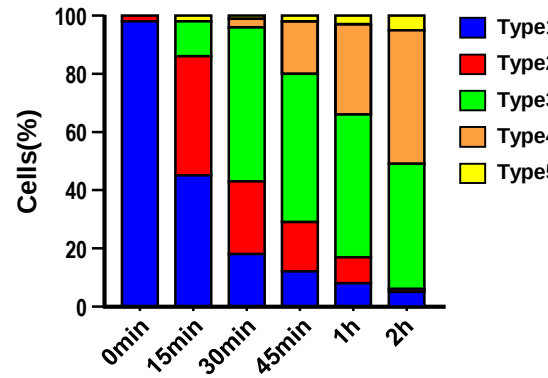

Figure. 3

A

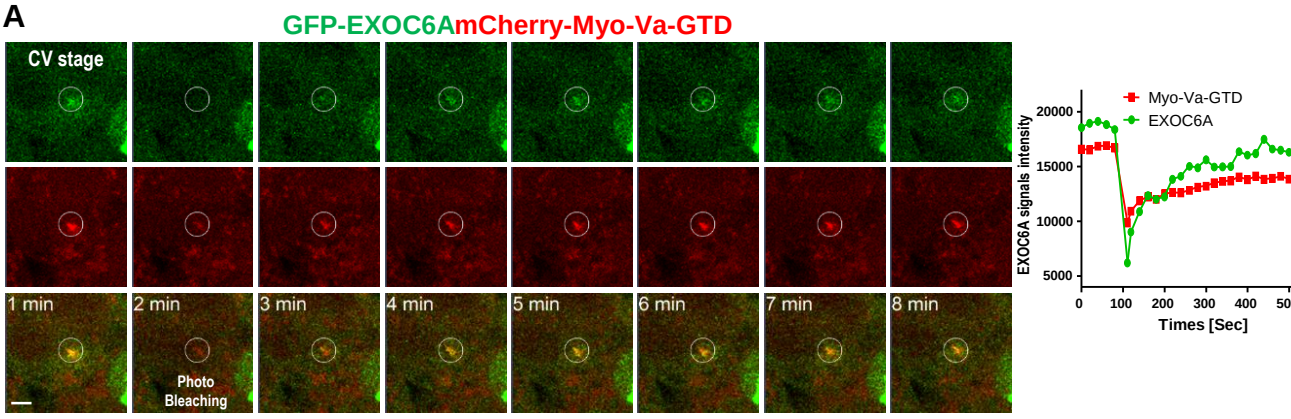

B

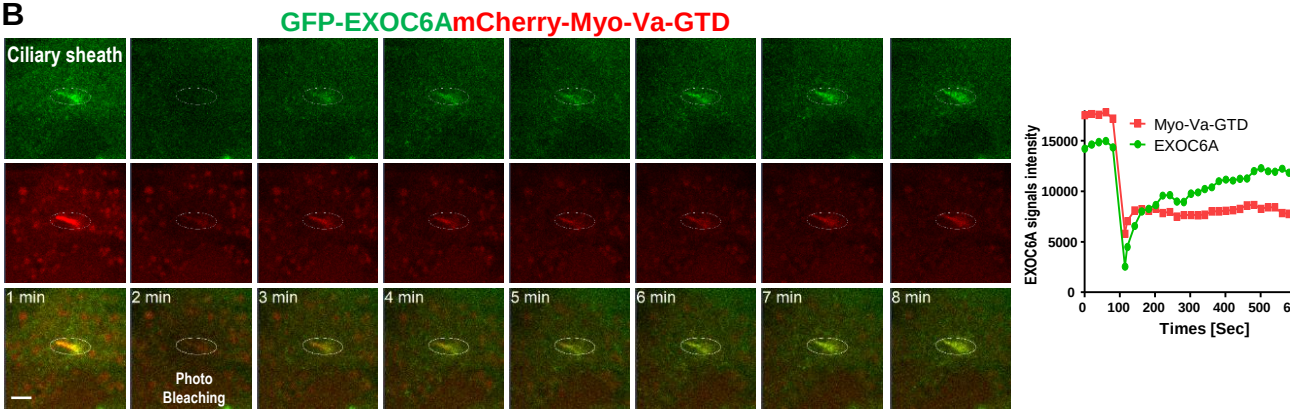

C

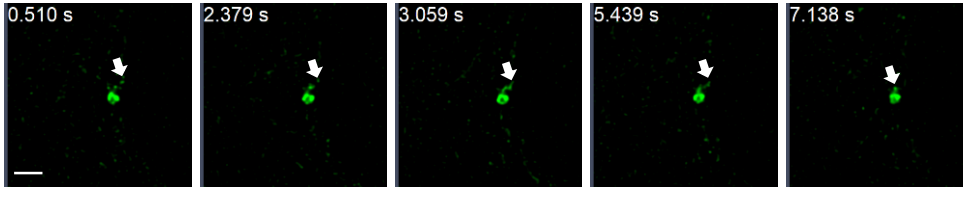

D

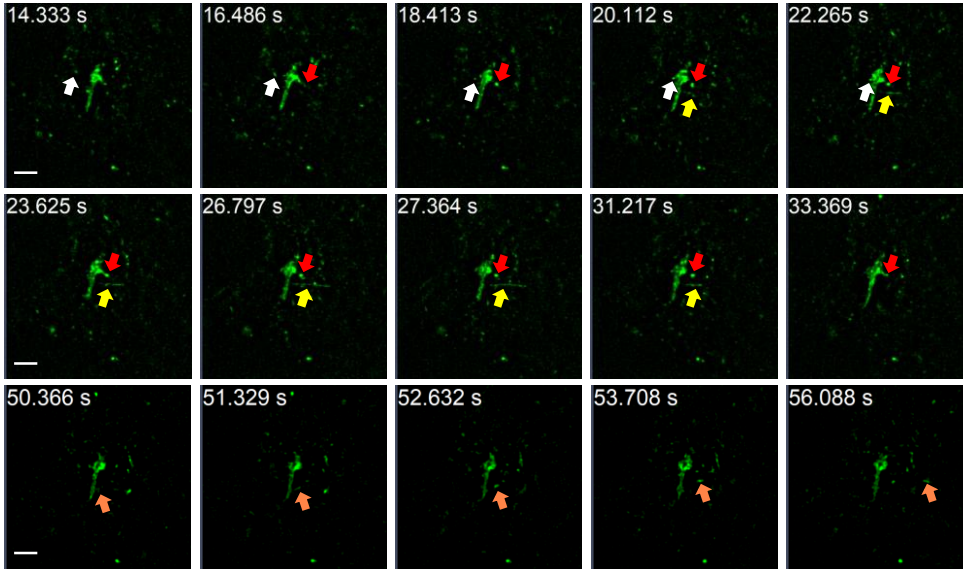

Figure. 4

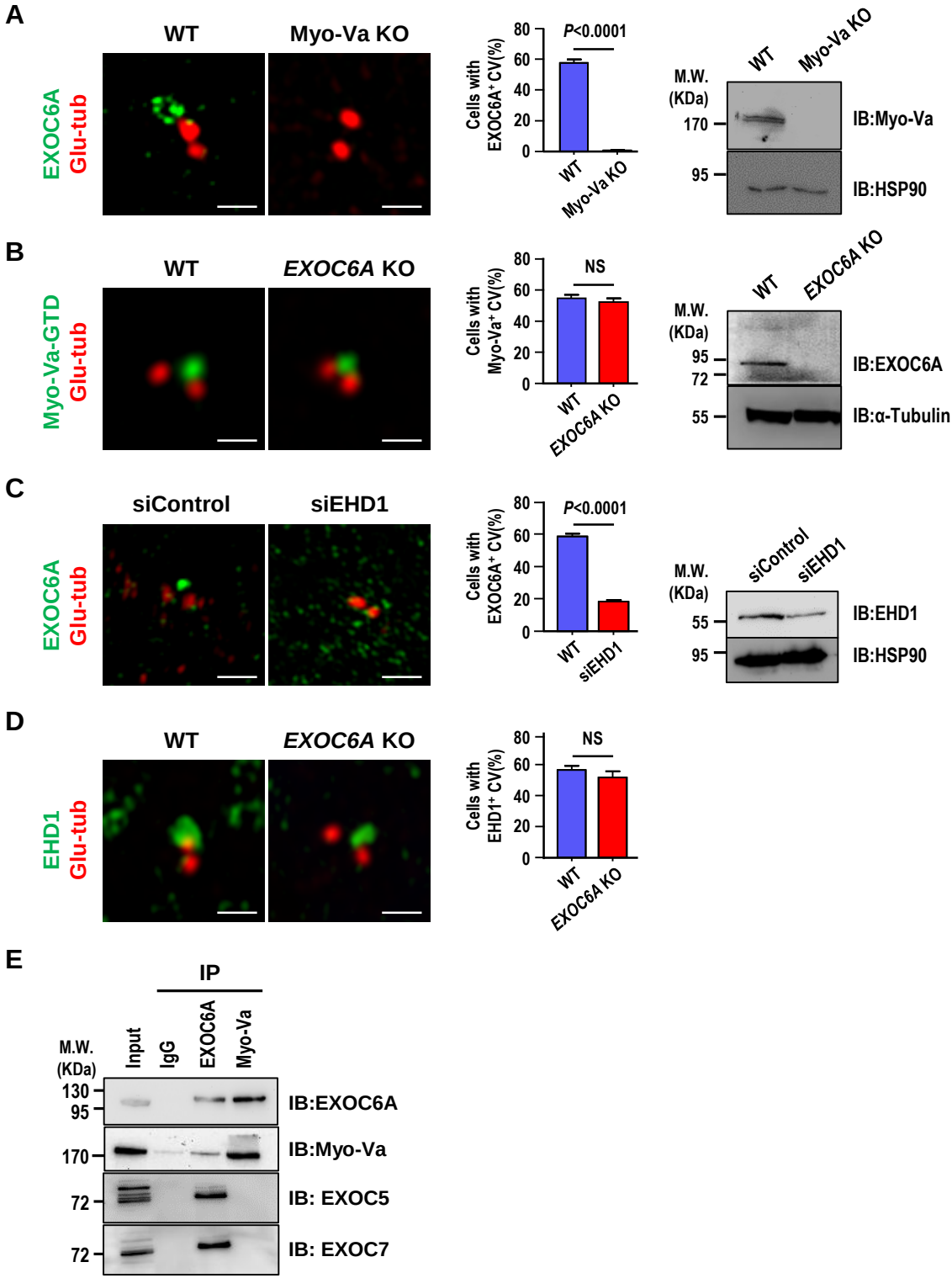
A
WT
Myo-Va KO
EXOC6A
Glu-tub
Cells with EXOC6A+ CV(%)
P<0.0001
WT
Myo-Va KO
M.W. (KDa)
170
95
IB:Myo-Va
IB:HSP90
B
WT
EXOC6A KO
Myo-Va-GTD
Glu-tub
Cells with Myo-Va+ CV(%)
NS
EXOC6A
IB:EXOC6A
IB:α-Tubulin
72
55
C
siControl
siEHD1
Cells with EXOC6A+ CV(%)
IB:EHD1
D
EHD1
Cells with EHD1+ CV(%)
E
IP
Input
IgG
130
IB: EXOC5
IB: EXOC7

Figure. 5

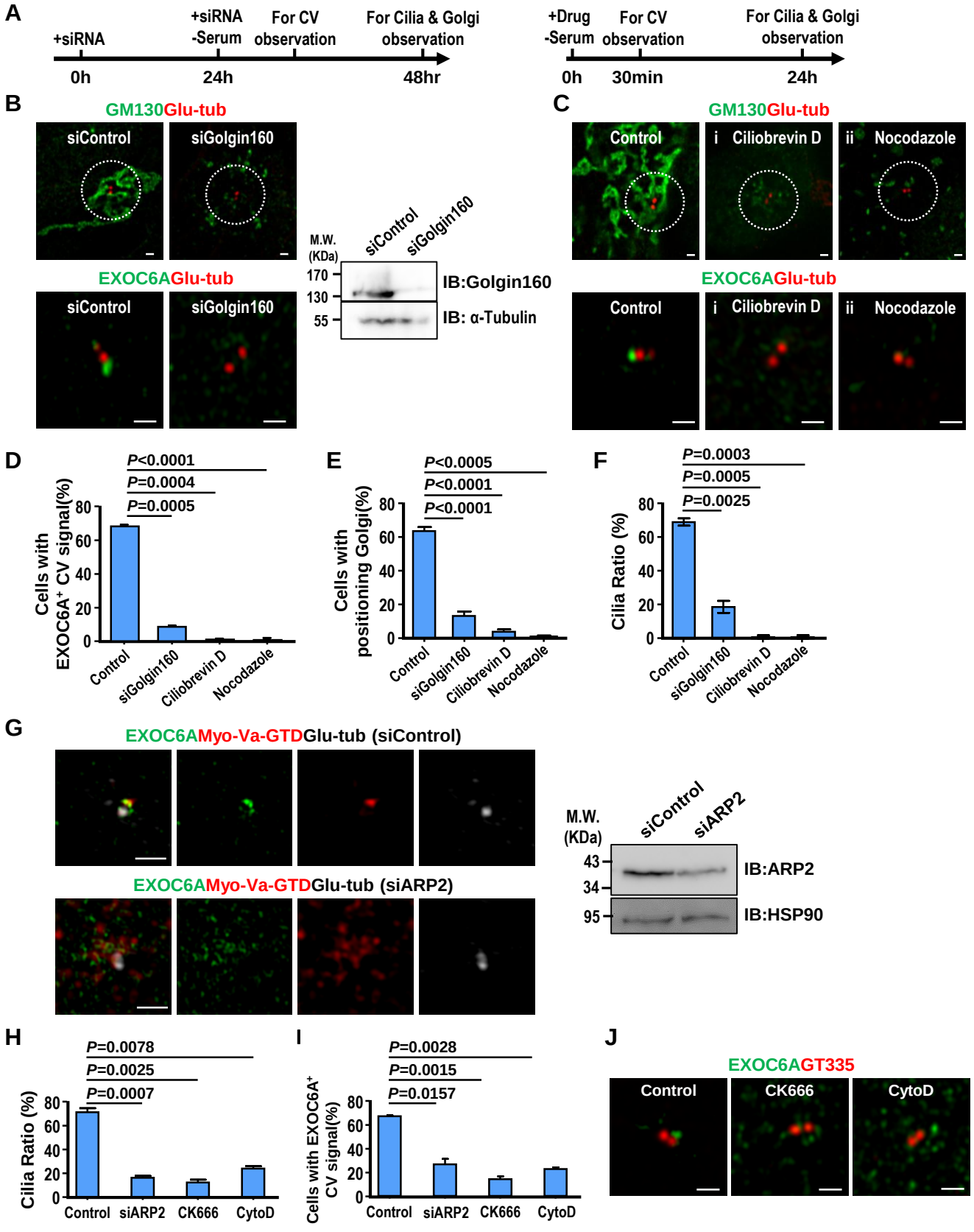
A
+siRNA
+siRNA -Serum
For CV observation
For Cilia & Golgi observation
0h
24h
48hr
+Drug -Serum
For CV observation
For Cilia & Golgi observation
0h
30min
24h
B
GM130Glu-tub
siControl
siGolgin160
EXOC6AGlu-tub
siControl
siGolgin160
M.W. (KDa)
siControl
siGolgin160
170
130
55
IB:Golgin160
IB: α-Tubulin
C
GM130Glu-tub
Control
i Ciliobrevin D
ii Nocodazole
EXOC6AGlu-tub
Control
i Ciliobrevin D
ii Nocodazole
D
P<0.0001
P=0.0004
P=0.0005
Cells with EXOC6A+ CV signal(%)
Control
siGolgin160
Ciliobrevin D
Nocodazole
E
P<0.0005
P<0.0001
P<0.0001
Cells with positioning Golgi(%)
Control
siGolgin160
Ciliobrevin D
Nocodazole
F
P=0.0003
P=0.0005
P=0.0025
Cilia Ratio (%)
Control
siGolgin160
Ciliobrevin D
Nocodazole
G
EXOC6AMyo-Va-GTDGlu-tub (siControl)
EXOC6AMyo-Va-GTDGlu-tub (siARP2)
M.W. (KDa)
siControl
siARP2
43
34
95
IB:ARP2
IB:HSP90
H
P=0.0078
P=0.0025
P=0.0007
Cilia Ratio (%)
Control
siARP2
CK666
CytoD
I
P=0.0028
P=0.0015
P=0.0157
Cells with EXOC6A+ CV signal(%)
Control
siARP2
CK666
CytoD
J
EXOC6AGT335
Control
CK666
CytoD

Figure. 6

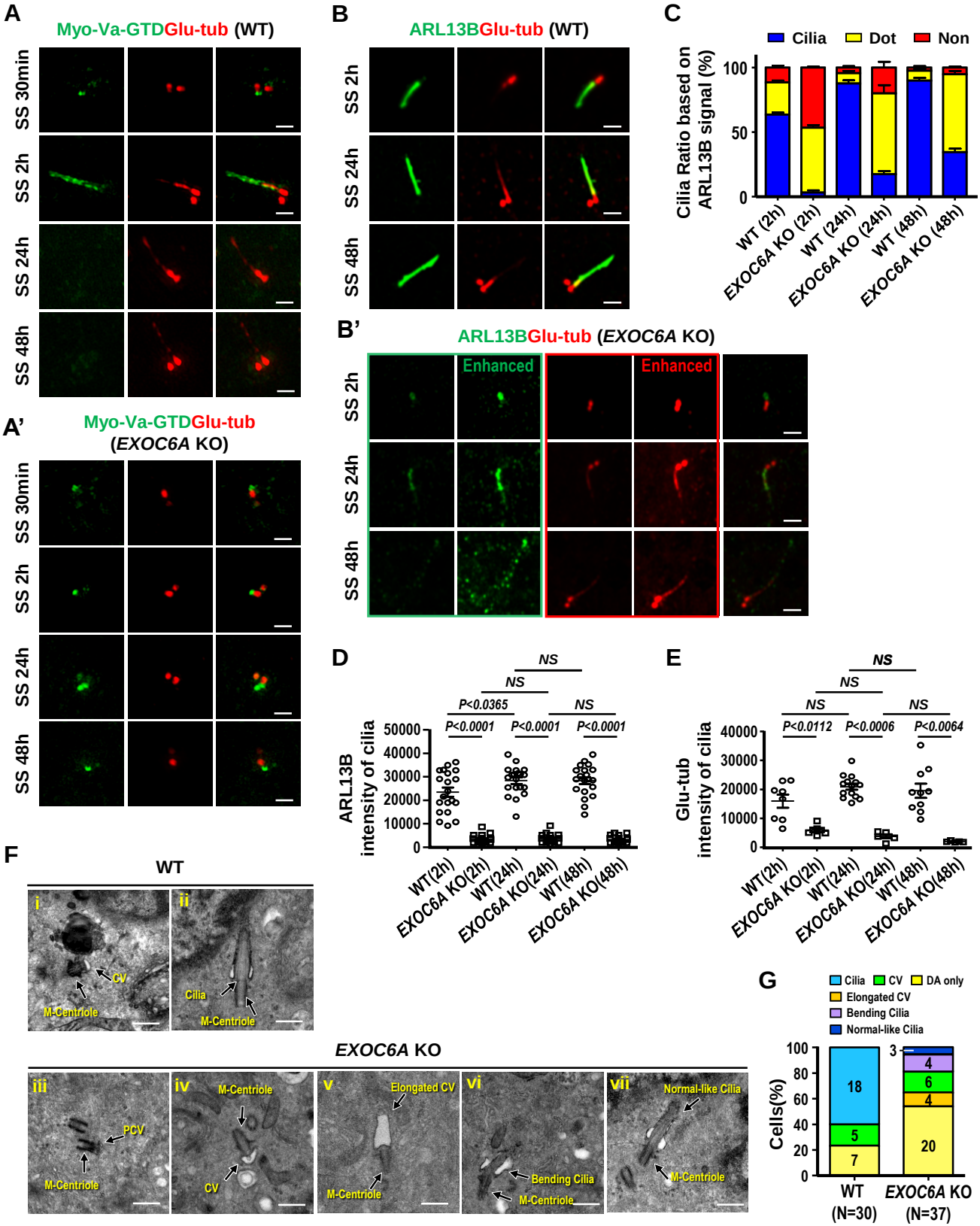
A
Myo-Va-GTDGlu-tub (WT)
SS 30min
SS 2h
SS 24h
SS 48h
A'
Myo-Va-GTDGlu-tub
(EXOC6A KO)
SS 30min
SS 2h
SS 24h
SS 48h
B
ARL13BGlu-tub (WT)
SS 2h
SS 24h
SS 48h
B'
ARL13BGlu-tub (EXOC6A KO)
Enhanced
Enhanced
SS 2h
SS 24h
SS 48h
C
Cilia
Dot
Non
Cilia Ratio based on ARL13B signal (%)
100
50
0
WT (2h)
EXOC6A KO (2h)
WT (24h)
EXOC6A KO (24h)
WT (48h)
EXOC6A KO (48h)
D
NS
NS
P<0.0365
NS
P<0.0001
P<0.0001
P<0.0001
ARL13B intensity of cilia
50000
40000
30000
20000
10000
0
WT(2h)
EXOC6A KO(2h)
WT(24h)
EXOC6A KO(24h)
WT(48h)
EXOC6A KO(48h)
E
NS
NS
NS
NS
P<0.0112
P<0.0006
P<0.0064
Glu-tub intensity of cilia
40000
30000
20000
10000
0
WT(2h)
EXOC6A KO(2h)
WT(24h)
EXOC6A KO(24h)
WT(48h)
EXOC6A KO(48h)
F
WT
i
CV
M-Centriole
ii
Cilia
M-Centriole
EXOC6A KO
iii
PCV
M-Centriole
iv
M-Centriole
CV
v
Elongated CV
M-Centriole
vi
Bending Cilia
M-Centriole
vii
Normal-like Cilia
M-Centriole
G
Cilia
CV
DA only
Elongated CV
Bending Cilia
Normal-like Cilia
Cells(%)
100
80
60
40
20
0
18
5
7
3
4
6
4
20
WT
(N=30)
EXOC6A KO
(N=37)

Figure. 7

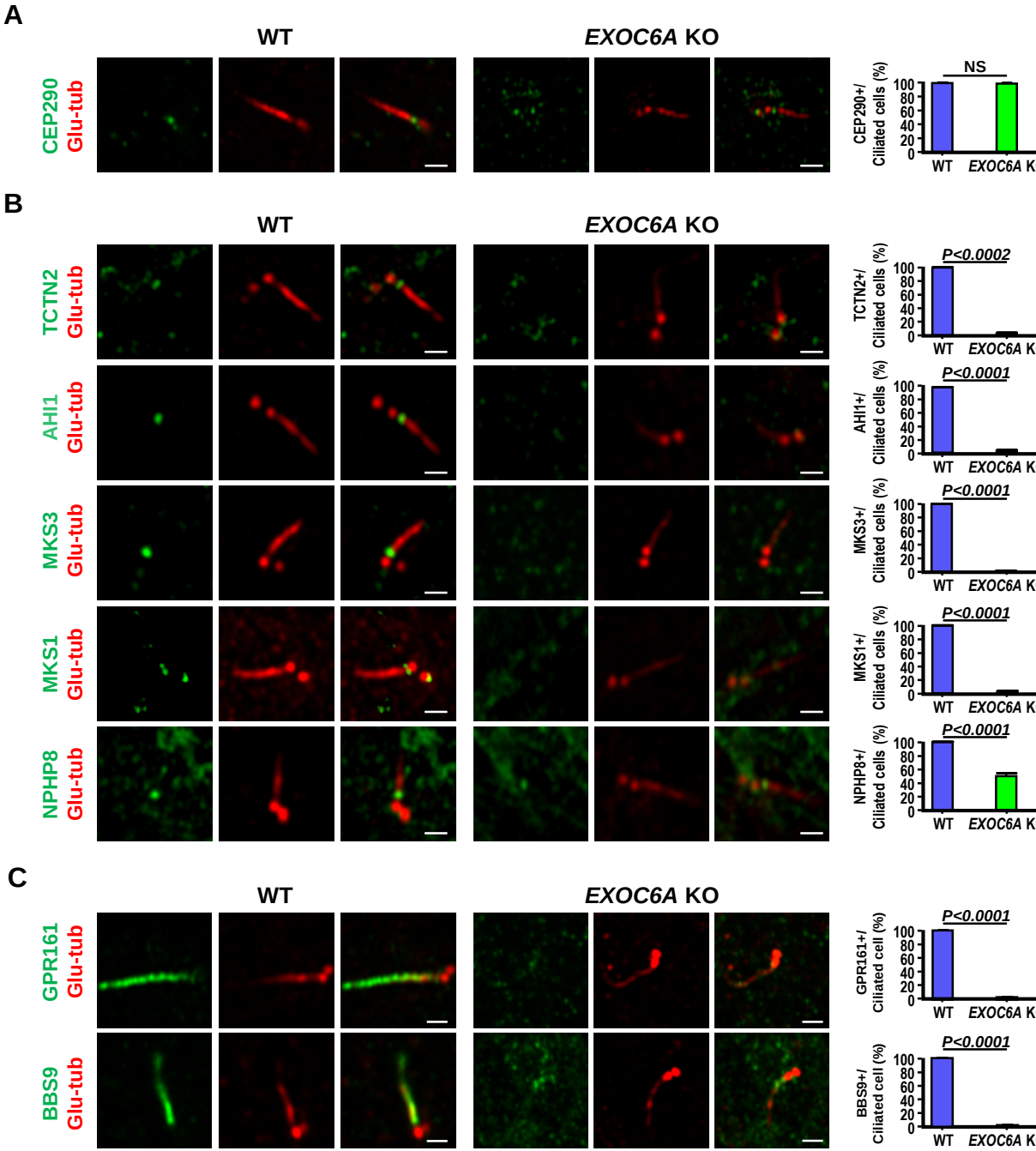
A
WT
EXOC6A KO
CEP290
Glu-tub
NS
CEP290+/ Ciliated cells (%)
WT
EXOC6A KO
B
WT
EXOC6A KO
TCTN2
Glu-tub
P<0.0002
TCTN2+/ Ciliated cells (%)
AHI1
Glu-tub
P<0.0001
AHI1+/ Ciliated cells (%)
MKS3
Glu-tub
P<0.0001
MKS3+/ Ciliated cells (%)
MKS1
Glu-tub
P<0.0001
MKS1+/ Ciliated cells (%)
NPHP8
Glu-tub
P<0.0001
NPHP8+/ Ciliated cells (%)
C
WT
EXOC6A KO
GPR161
Glu-tub
P<0.0001
GPR161+/ Ciliated cell (%)
BBS9
Glu-tub
P<0.0001
BBS9+/ Ciliated cell (%)

Figure. 8

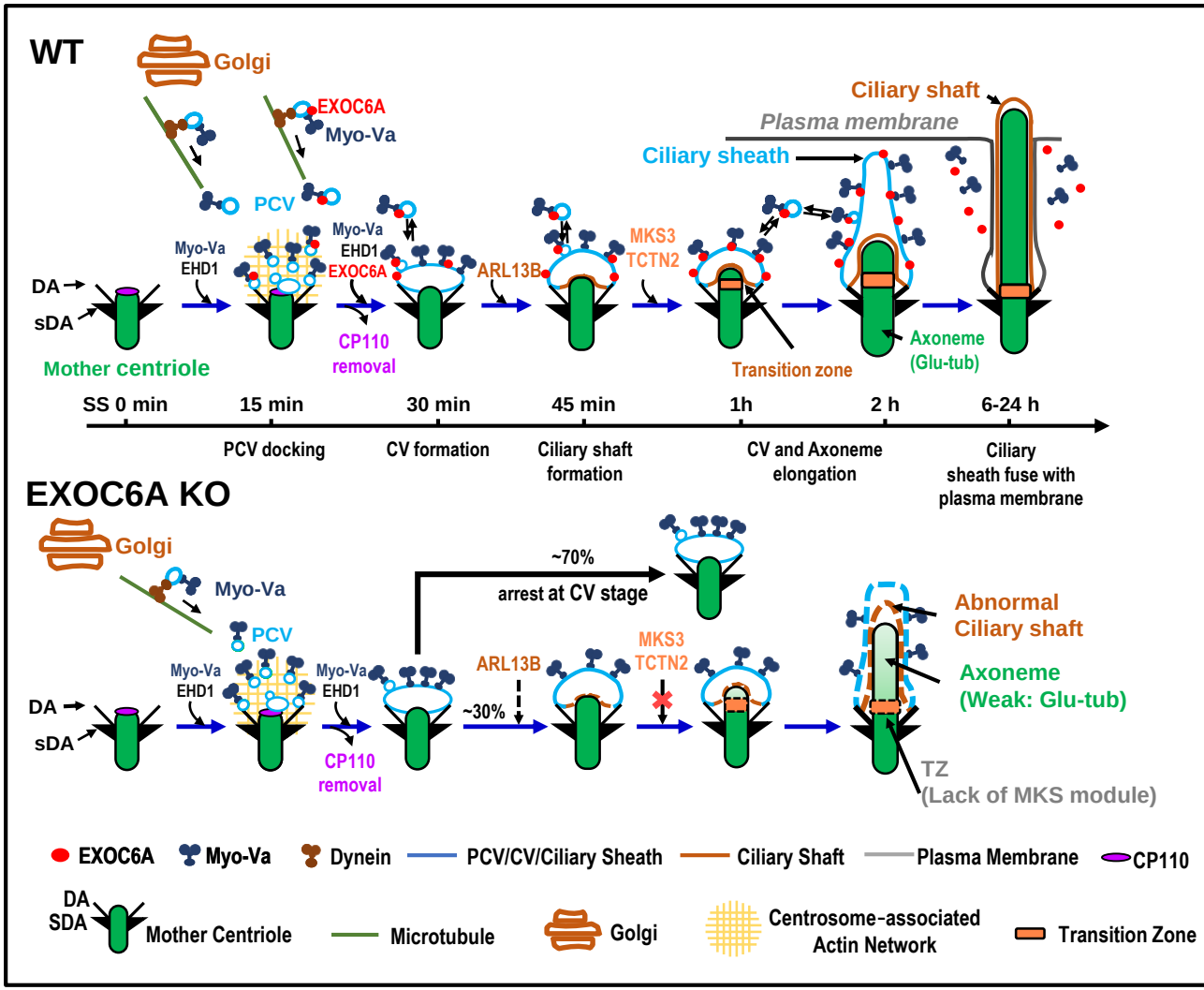
WT
Golgi
EXOC6A
Myo-Va
PCV
Ciliary shaft
Plasma membrane
Ciliary sheath
Myo-Va
EHD1
Myo-Va
EHD1
EXOC6A
ARL13B
MKS3
TCTN2
DA
sDA
Mother centriole
CP110
removal
Transition zone
Axoneme
(Glu-tub)
SS 0 min
15 min
30 min
45 min
1h
2 h
6-24 h
PCV docking
CV formation
Ciliary shaft
formation
CV and Axoneme
elongation
Ciliary
sheath fuse with
plasma membrane
EXOC6A KO
Golgi
Myo-Va
PCV
~70%
arrest at CV stage
Abnormal
Ciliary shaft
Axoneme
(Weak: Glu-tub)
Myo-Va
EHD1
Myo-Va
EHD1
ARL13B
~30%
MKS3
TCTN2
DA
sDA
CP110
removal
TZ
(Lack of MKS module)
EXOC6A
Myo-Va
Dynein
PCV/CV/Ciliary Sheath
Ciliary Shaft
Plasma Membrane
CP110
DA
SDA
Mother Centriole
Microtubule
Golgi
Centrosome-associated
Actin Network
Transition Zone

Supplementary Figure 1

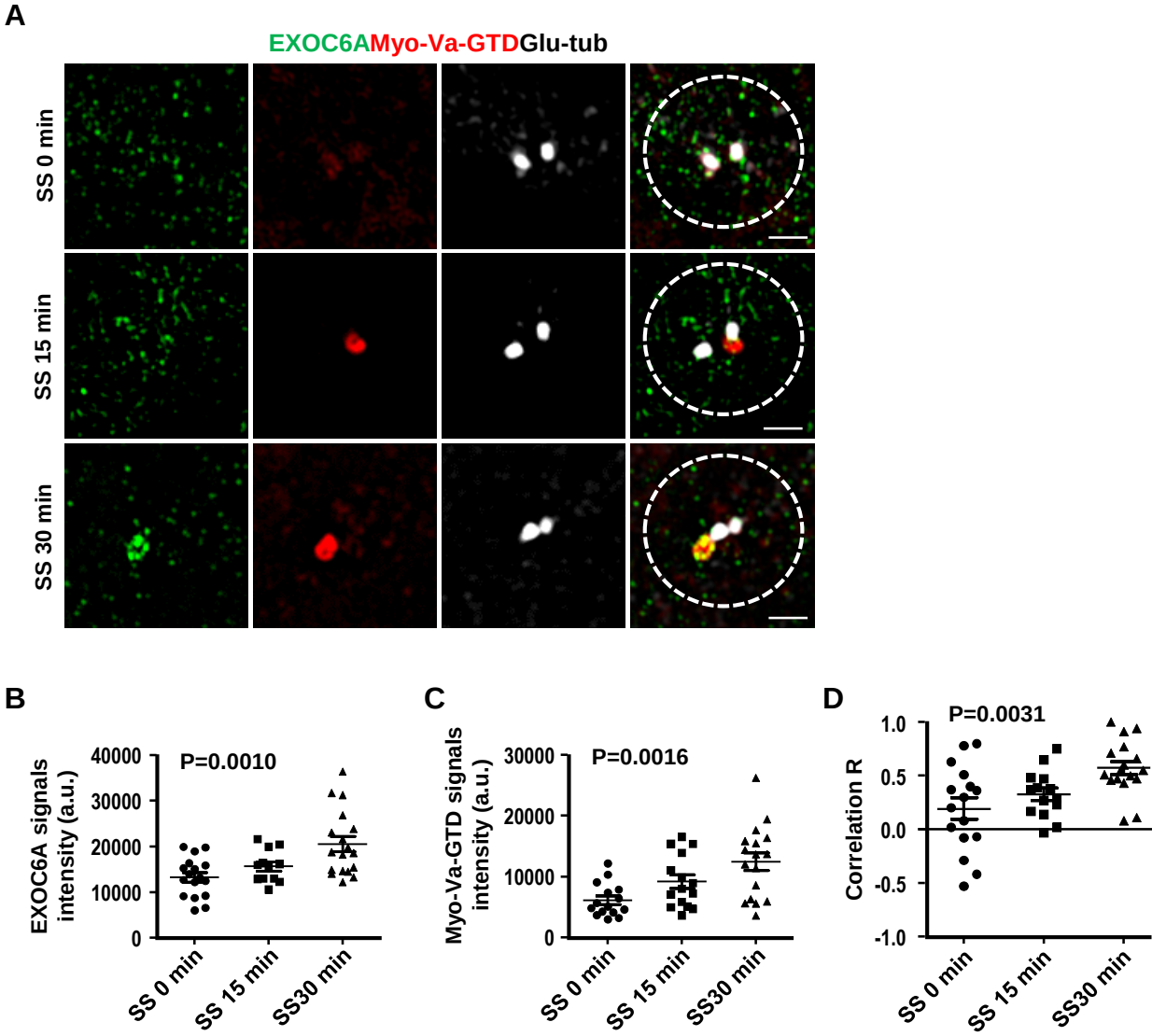

Supplementary Figure 2

A

GFP-EXOC6AmCherry-MyoVa-GTDSir-tubulin

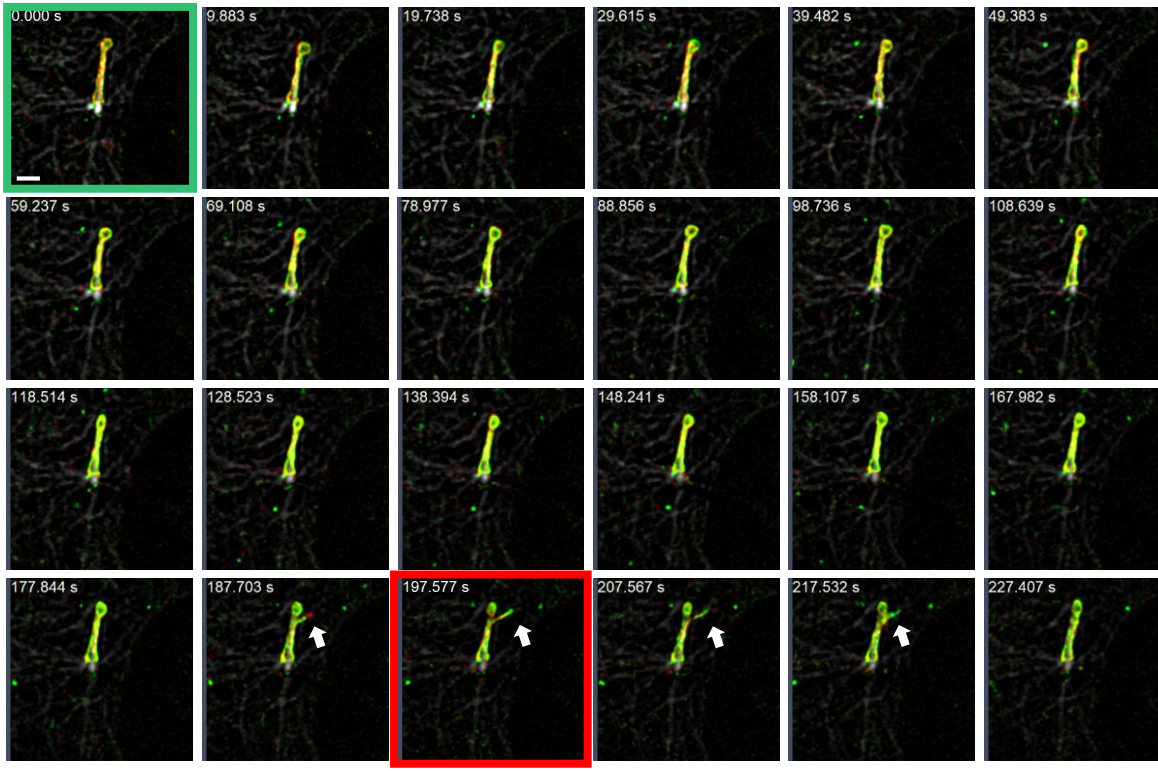

B

GFP-EXOC6AmCherry-MyoVa-GTDSir-tubulin

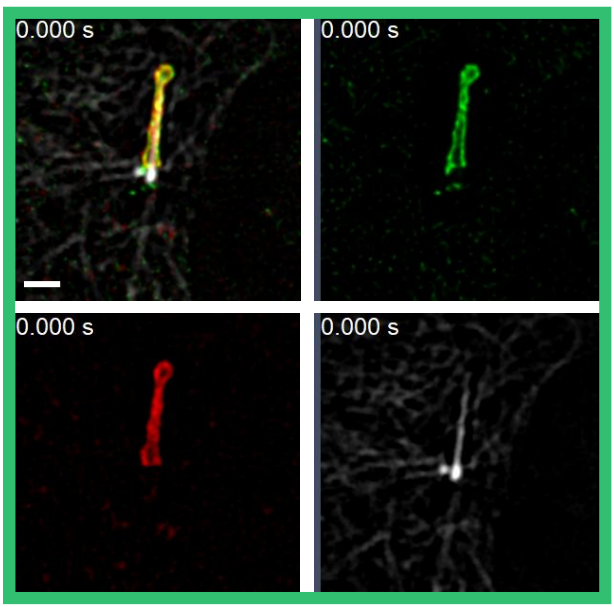

C

GFP-EXOC6AmCherry-MyoVa-GTDSir-tubulin

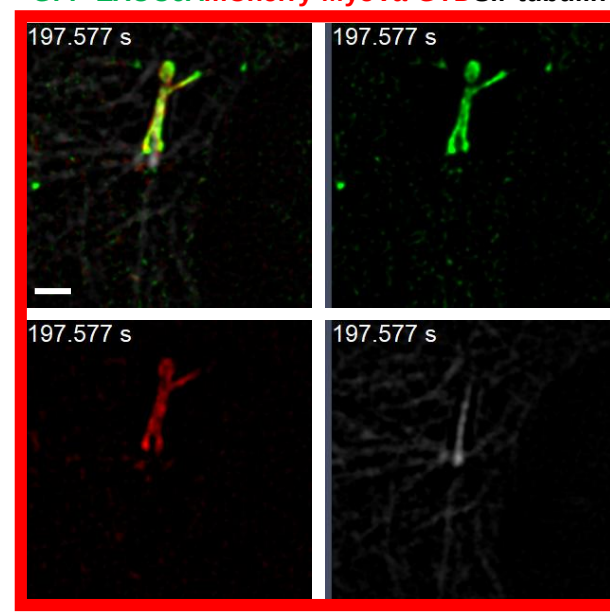

Supplementary Figure 3

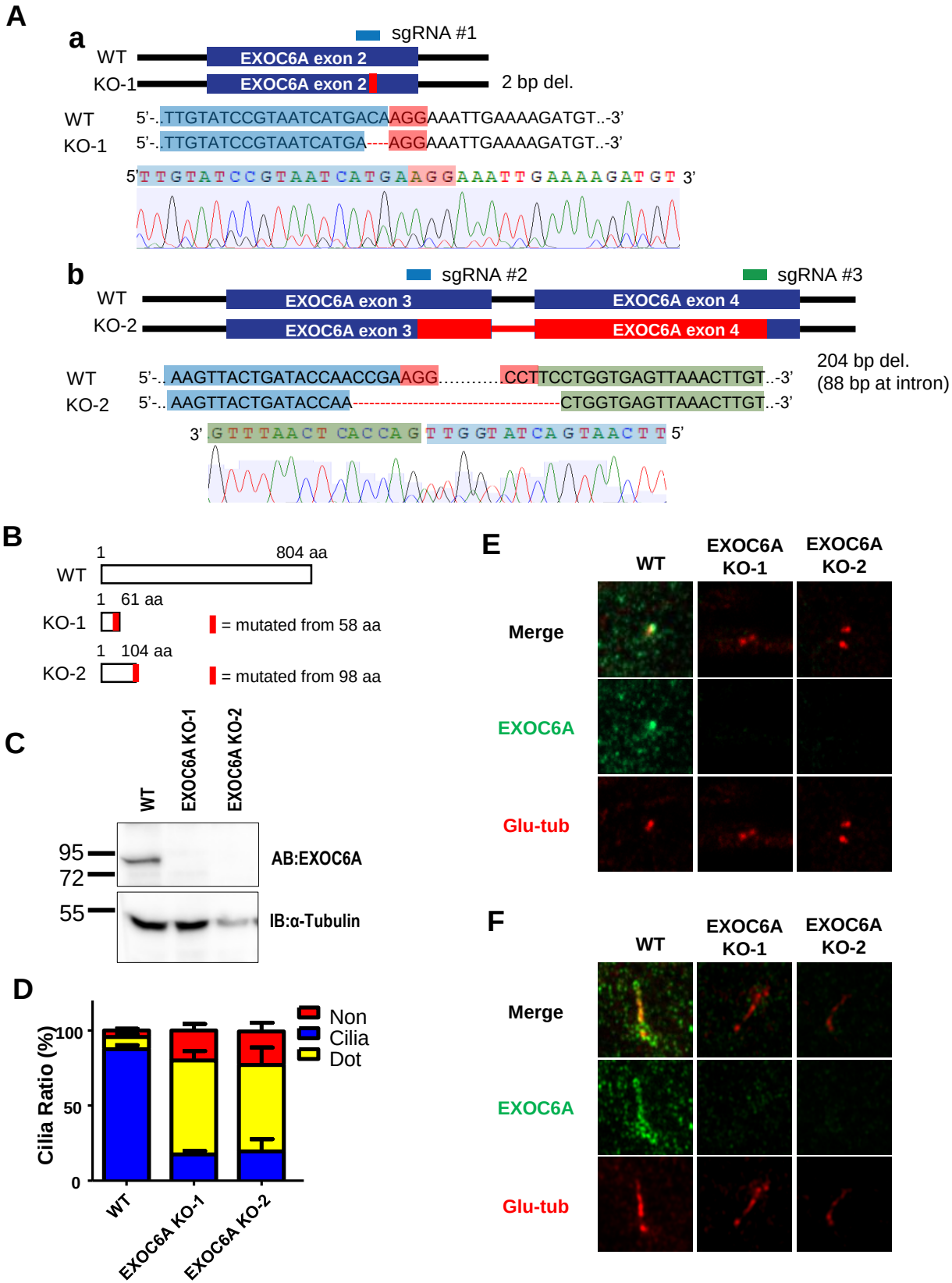

Supplementary Figure 4

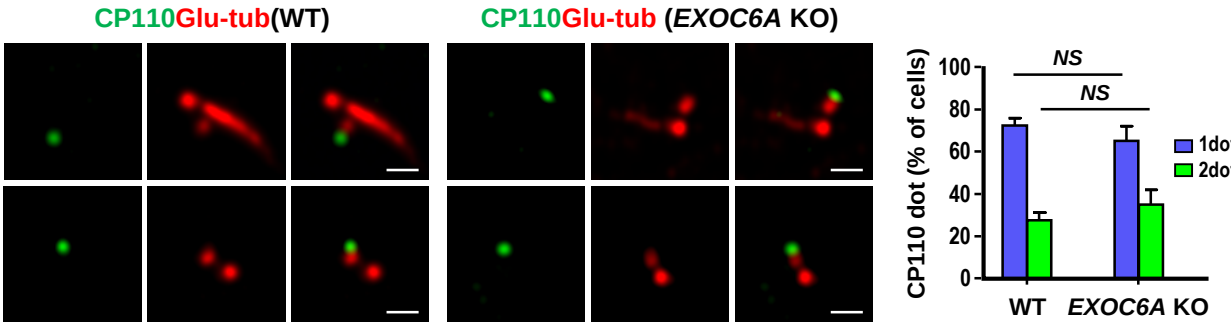

Supplementary Figure 5

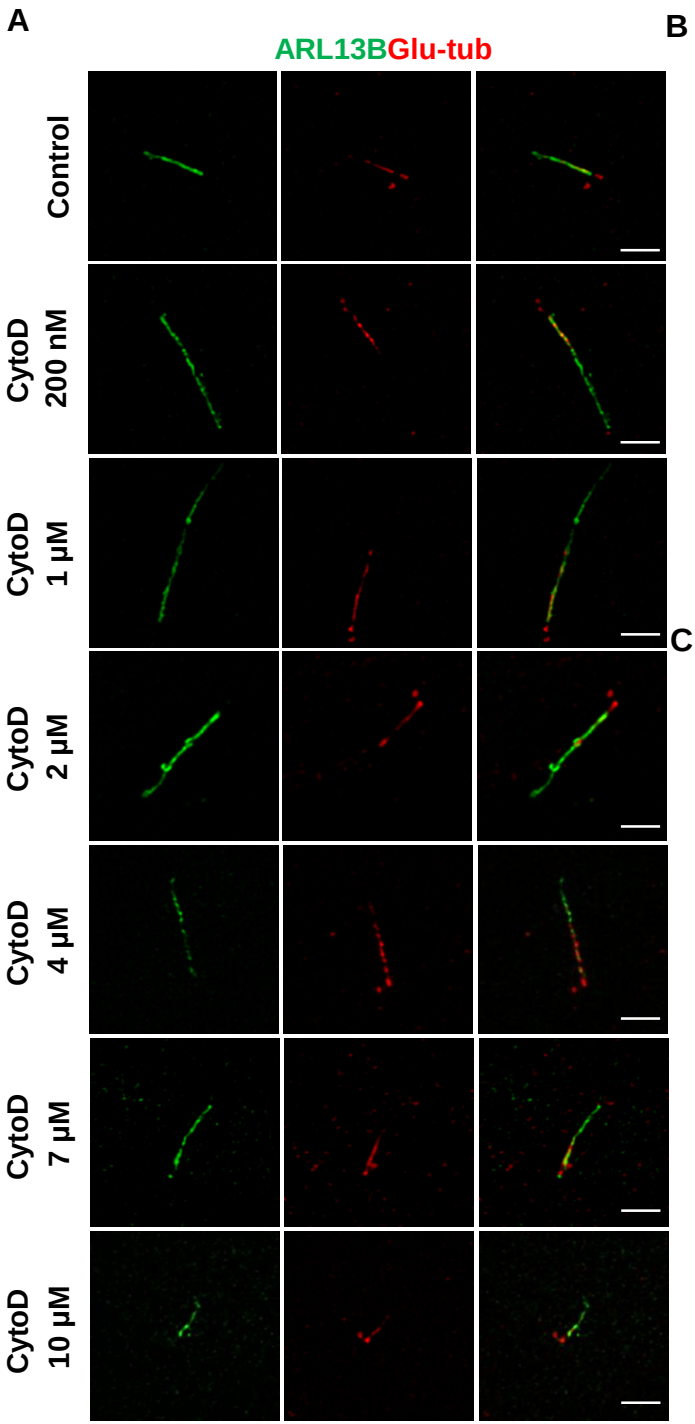

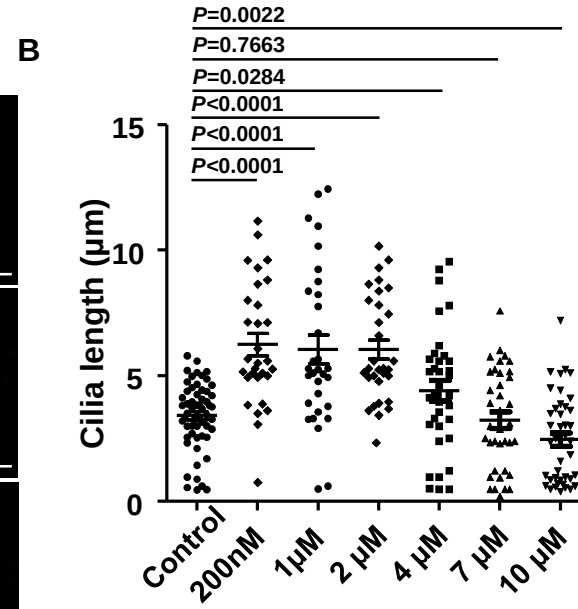

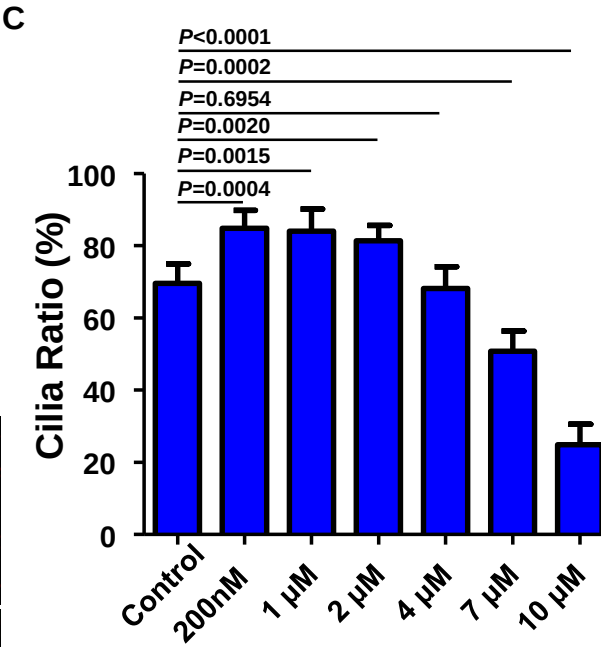

Supplementary Figure 6

A

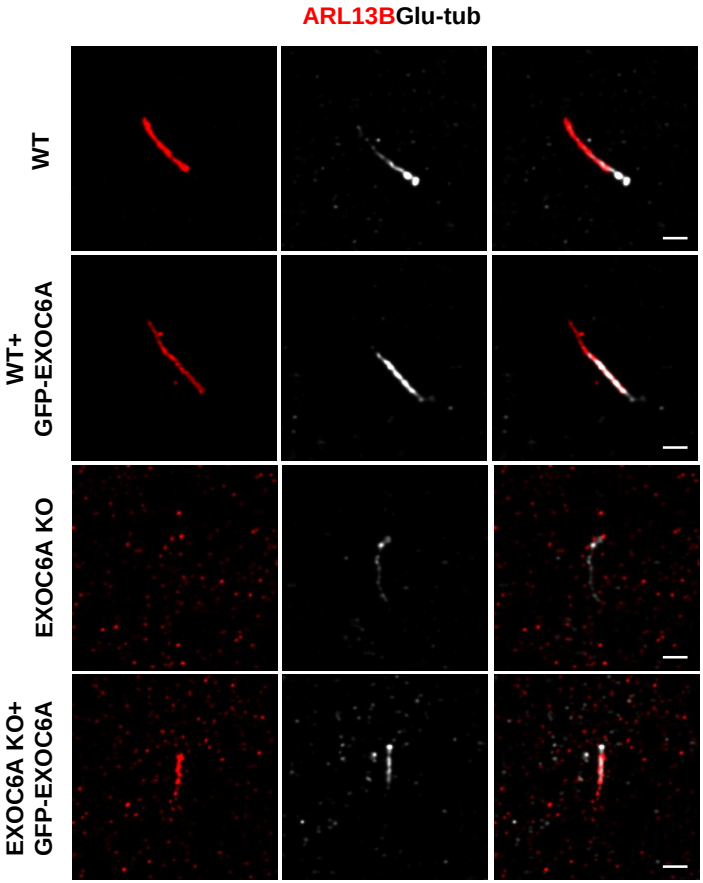

B

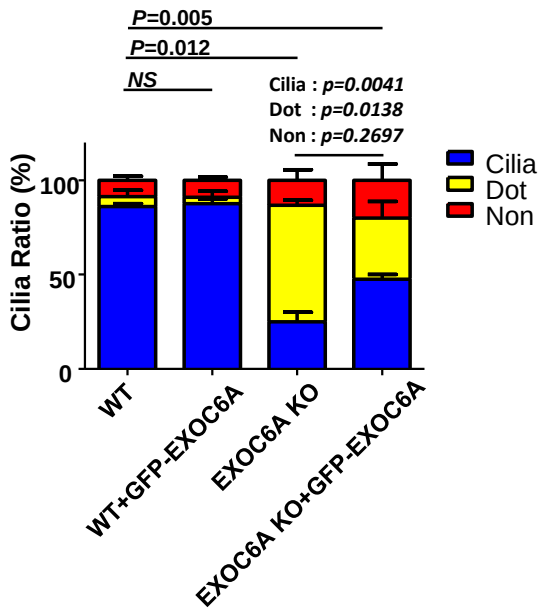

Source Data

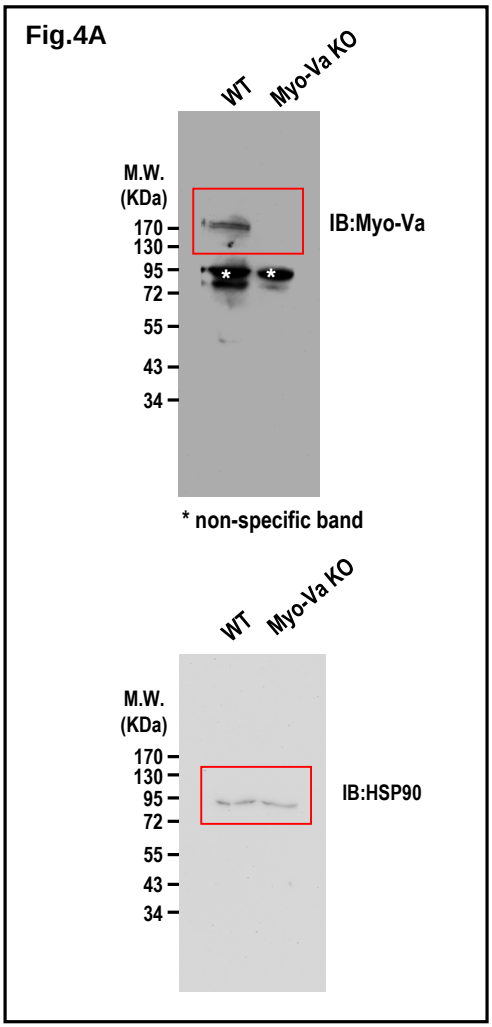
Fig.4A
WT
Myo-Va KO
M.W.
(KDa)
170
130
95
72
55
43
34
IB:Myo-Va
* non-specific band
WT
Myo-Va KO
M.W.
(KDa)
170
130
95
72
55
43
34
IB:HSP90

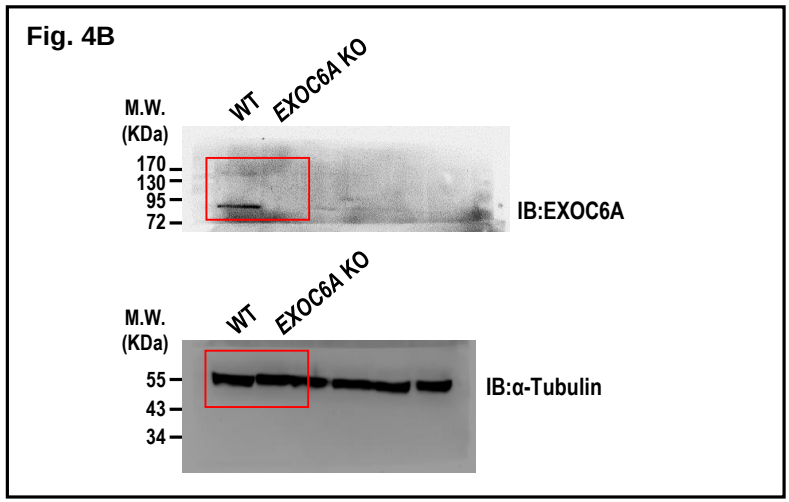
Fig. 4B
M.W.
(KDa)
WT
EXOC6A KO
170
130
95
72
IB:EXOC6A
M.W.
(KDa)
WT
EXOC6A KO
55
43
34
IB:α-Tubulin

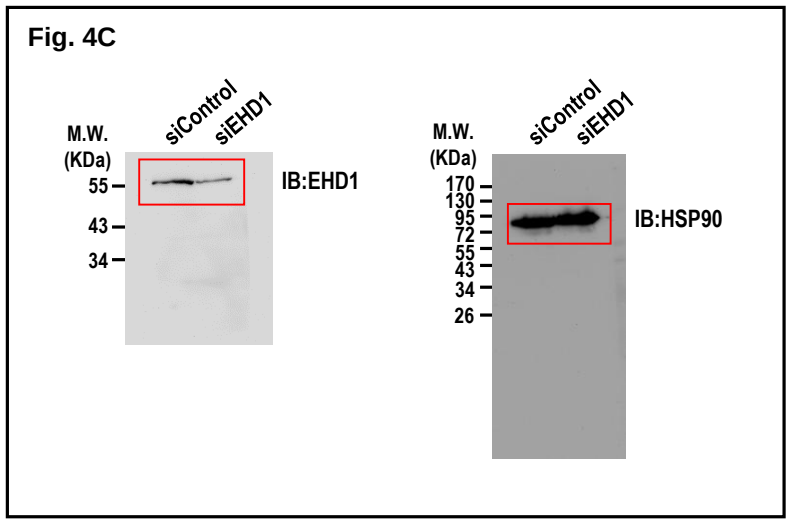
Fig. 4C
M.W.
(KDa)
siControl
siEHD1
55
43
34
IB:EHD1
M.W.
(KDa)
siControl
siEHD1
170
130
95
72
55
43
34
26
IB:HSP90

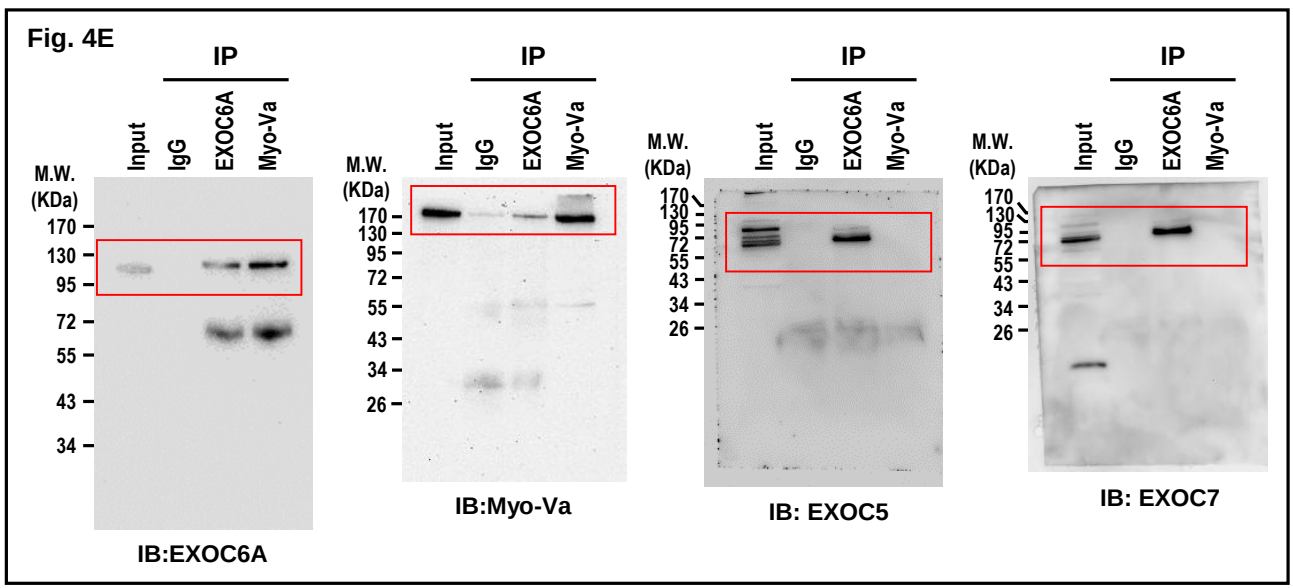
Fig. 4E
IP
Input
IgG
EXOC6A
Myo-Va
M.W.
(KDa)
170
130
95
72
55
43
34
IB:EXOC6A
IP
Input
IgG
EXOC6A
Myo-Va
M.W.
(KDa)
170
130
95
72
55
43
34
26
IB:Myo-Va
IP
Input
IgG
EXOC6A
Myo-Va
M.W.
(KDa)
170
130
95
72
55
43
34
26
IB: EXOC5
IP
Input
IgG
EXOC6A
Myo-Va
M.W.
(KDa)
170
130
95
72
55
43
34
26
IB: EXOC7

Source Data

Fig. 5B

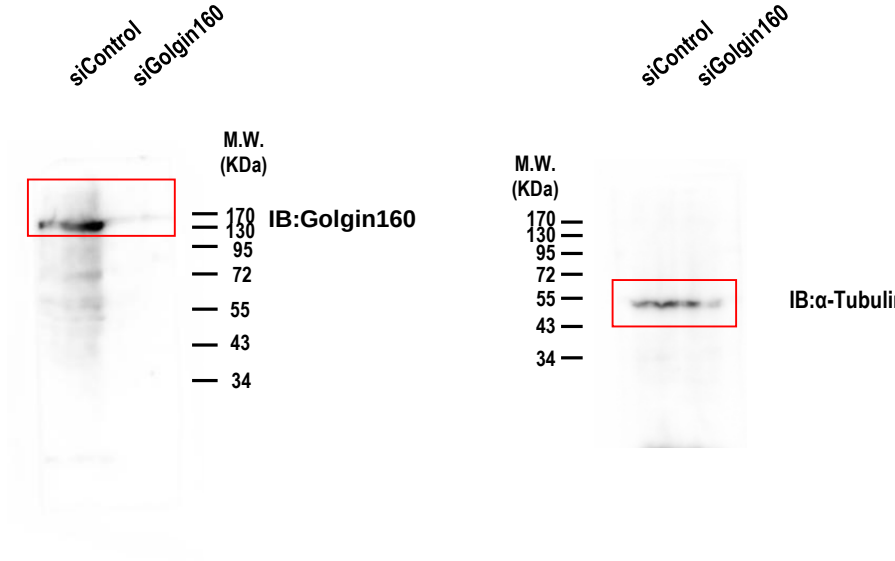

Fig. 5G

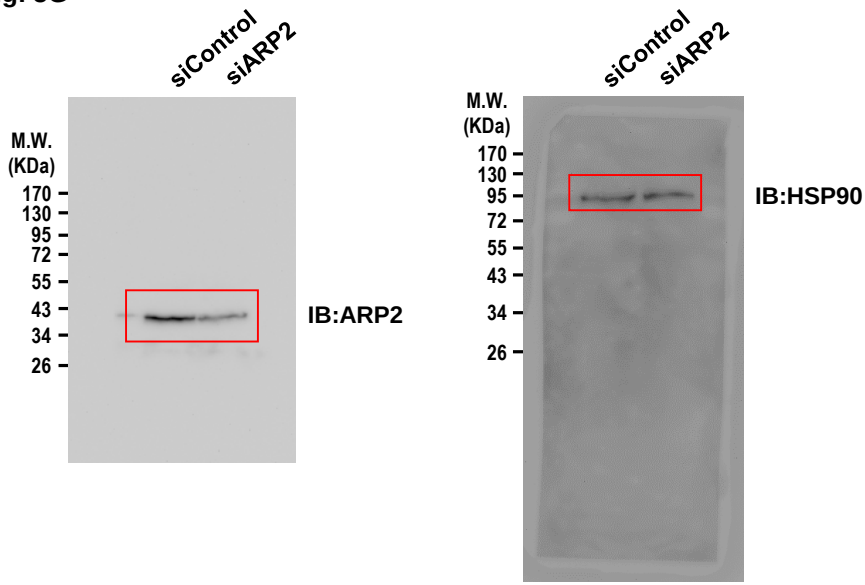

Source Data
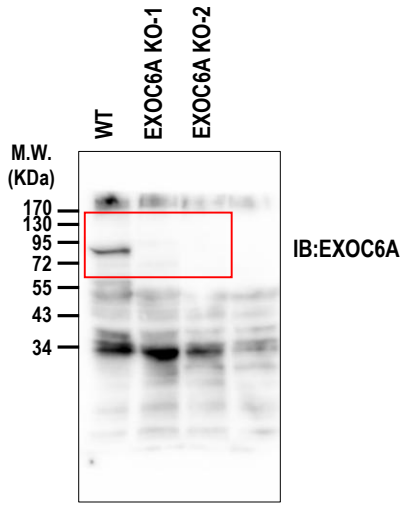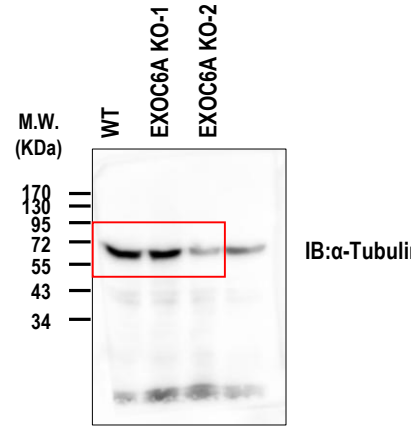
Fig. S3C